

1 Spatially varying cis-regulatory 2 divergence in *Drosophila* embryos 3 elucidates cis-regulatory logic

4 Peter A. Combs^{1*} and Hunter B. Fraser^{1*}

*For correspondence:

pcombs@stanford.edu (PAC);
hbfraser@stanford.edu (HBF)

5 ¹Department of Biology, Stanford University, Stanford, CA

6

7 **Abstract** Spatial patterning of gene expression is a key process in development—responsible for
8 the incredible diversity of animal body plans—yet how it evolves is still poorly understood. Both cis-
9 and trans-acting changes could accumulate and participate in complex interactions, so to isolate
10 the cis-regulatory component of patterning evolution, we measured allele-specific spatial gene
11 expression patterns in *D. melanogaster* × *D. simulans* hybrid embryos. RNA-seq of cryosectioned
12 slices revealed 55 genes with strong spatially varying allele-specific expression, and several
13 hundred more with weaker but significant spatial divergence. For example, we found that
14 *hunchback* (*hb*), a major regulator of developmental patterning, had reduced expression specifically
15 in the anterior tip of *D. simulans* embryos. Mathematical modeling of *hb* cis-regulation suggested
16 that a mutation in a Bicoid binding site was responsible, which we verified using CRISPR-Cas9
17 genome editing. In sum, even comparing morphologically near-identical species we identified a
18 substantial amount of spatial variation in gene expression, suggesting that development is robust
19 to many such changes, but also that natural selection may have ample raw material for evolving
20 new body plans via cis-regulatory divergence.

21

22 Introduction

23 Although most cells in any metazoan share the same genome, they nevertheless diversify into
24 an impressive variety of precisely localized cell types during development. This complex spatial
25 patterning is due to the precise expression of genes at different locations and times during develop-
26 ment. Where and when each gene is expressed is largely dictated by the activities of cis-regulatory
27 modules (CRMs, also sometimes called enhancers) through the binding of transcription factors to
28 their recognition sequences (*Banerji et al., 1981; Ptashne, 1986; Driever et al., 1989*). Despite the
29 importance of these patterning CRMs for proper organismal development, they are able to tolerate
30 some modest variation in sequence and level of activity (*Ludwig and Kreitman, 1995; Lusk and*
31 *Eisen, 2010; Villar et al., 2015; Berthelot et al., 2017*). Indeed, this variation is one of the substrates
32 upon which selection can act. However, even in the handful of cases where we understand the
33 regulatory logic, efforts to predict the result of inter-specific differences in CRMs still have limited
34 precision (*Small et al., 1991; Samee and Sinha, 2014; Sayal et al., 2016*).

35 A complicating factor in comparing gene expression between species is that both cis- and
36 trans-acting regulation can change (*Coolon et al., 2014*). One solution is to focus on cis-regulatory
37 changes by measuring allele-specific expression (ASE) in F1 hybrids. In a hybrid each diploid
38 nucleus has one copy of each parent's genome which is exposed to the same trans-environment,
39 so any differences in zygotic usage of the two copies is due either to cis-regulatory divergence
40 or to stochastic bursting (which should be averaged out over many cells). The early *Drosophila*
41 embryo provides a unique opportunity to probe the interaction of trans-regulatory environments

42 with cis-regulatory sequence: by slicing the embryo along the anterior-posterior axis, we are able
43 to measure ASE in nuclei with similar complements of transcription factors (TFs). By combining
44 knowledge of both the regulatory sequence changes between the species and the transcription
45 factors expressed in each slice, it should be possible to more quickly identify which TF binding site
46 underlies the expression difference.

47 In this study, we used spatially-resolved transcriptome profiling to search for genes where
48 cis-regulatory differences drive allele-specific expression patterns in hybrid *D. melanogaster* × *D.*
49 *simulans* embryos (specifically the reference strains DGRP line 340 for *D. melanogaster* and *w*⁵⁰¹
50 for *D. simulans*; we will refer specifically to the two reference strains, and not the two species as
51 a whole unless otherwise noted). We found dozens of genes with clear, consistent differences in
52 allele-specific expression across the embryo. We chose one of these genes, *hunchback* (*hb*), as a
53 model to understand which of 17 polymorphisms in its regulatory regions was likely to drive the
54 expression difference. Mathematical modeling of *hunchback* cis-regulation suggested that a Bicoid
55 binding site change was responsible for the expression difference, which we confirmed through
56 CRISPR-Cas9 mediated editing of the endogenous *D. melanogaster* locus.

57 Results

58 A genome-wide atlas of spatial gene expression in *D. melanogaster* × *D. simulans* 59 hybrids

60 We selected five mid-stage 5 hybrid embryos, with membrane invagination between 50 and 65%.
61 We then sliced the embryos to a resolution of 14μ, yielding between 24 and 27 slices per embryo.
62 We chose embryos from reciprocal crosses (i.e. with either a *D. melanogaster* mother or a *D. simulans*
63 mother), and had at least one embryo of each sex from each direction of the cross. Although hybrid
64 female embryos with a *D. simulans* mother are embryonic lethal at approximately this stage due
65 to a heterochromatin segregation defect (*Ferree and Barbash, 2009*), they were morphologically
66 normal and so we included one female embryo from this cross. We also sliced one embryo from
67 each of the parental strains. Following slicing, we amplified and sequenced poly-adenylated mRNA
68 using SMART-seq2 with minor modifications (*Combs, 2015; Picelli et al., 2014, 2013*).

69 We first searched for cases of hybrid mis-expression—genes where the absolute expression
70 pattern is consistently different in the hybrid, compared to the parents alone. Using earth-mover
71 distance (EMD) to measure differences in expression patterns (*Figure 1*—Figure supplement 2A;
72 *Rubner et al. (1998)*), for each zygotically expressed gene we compared the expression pattern from
73 each of the hybrid embryos to the pattern expected by taking the average of the *D. melanogaster*
74 and *D. simulans* embryos. After Benjamini-Hochberg FDR correction, no gene was significantly
75 more different from the average of the parental embryos than each of the parental embryos were
76 from each other (smallest q-value = .37, see Methods). We also compared expression patterns
77 between hybrid embryos with a *D. melanogaster* mother to those with a *D. simulans* mother, and
78 found that most differences seemed to be due to differing patterns of maternal deposition or noisy
79 expression (*Figure 1*—Figure supplement 3). Thus, we conclude that there do not seem to be any
80 expression patterns that are not explained by differences in the parents or that are unique to the
81 hybrid context.

82 Overall Allele-specific Expression

83 In order to measure cis-regulatory differences in expression, we calculated allele-specific expression
84 (ASE) scores for each gene in each slice (*Figure 1A*). The ASE score is the ratio of the difference
85 between the number of *D. simulans* and *D. melanogaster* reads and the sum of the reads,

$$ASE = \frac{n_{sim} - n_{mel}}{n_{sim} + n_{mel}} \quad (1)$$

86 and ranges between -1 (100% *D. melanogaster* expression) and 1 (100% *D. simulans* expression).

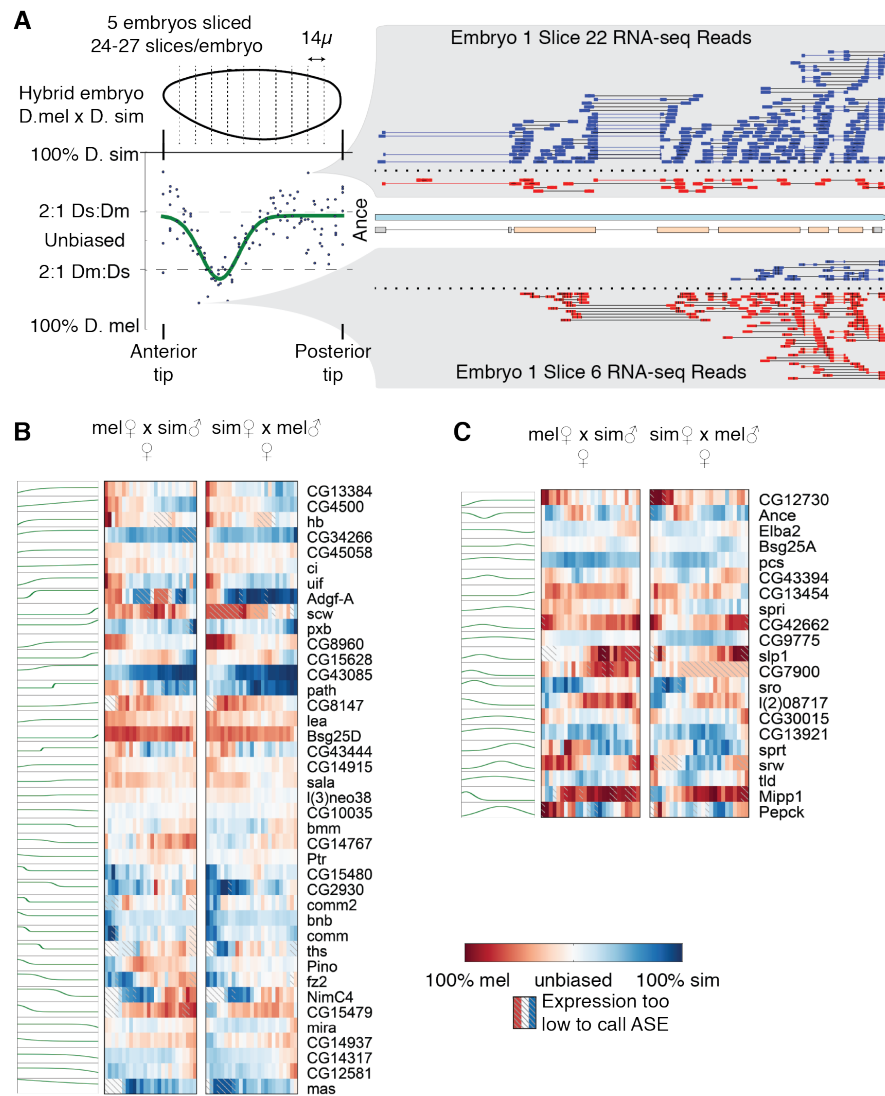


Figure 1. RNA-seq of hybrid *Drosophila* embryos reveals extensive spatially patterned allele-specific expression. A) Each embryo was cryosliced along the anterior-posterior axis in 14 μ sections, followed by RNA-seq in each slice. Allele-specific expression (ASE) was called for each gene in each slice by assigning unambiguous reads to the parent of origin; shown here are the reads for the gene *Ance*, with blue indicating *D. simulans* reads and red indicating *D. melanogaster* reads. For each gene, we fit either a step-like or peak-like (shown) function. B-C) Genes with a step-like pattern (B, best fit by a logistic function) or peak-like pattern (C, best fit by a Gaussian function). For each gene, anterior is left and posterior is right. The green line indicates the best fit pattern, with higher indicating *D. simulans* biased expression, and lower indicating *D. melanogaster* biased expression. The heatmaps are from two of the five embryos.

Figure 1—source data 1. Table of ASE values in each slice

Figure 1—Figure supplement 1. Summary data for embryos used

Figure 1—Figure supplement 2. Using earth mover distance to identify genes with different expression patterns between the hybrids and the parents

Figure 1—Figure supplement 3. Using earth mover distance to identify genes with different expression patterns between the directions of the hybrid cross

Figure 1—source data 2. Table of absolute expression values in each slice, used for comparing patterning differences in Figure 1—Figure supplement 2

Figure 1—Figure supplement 4. Complete heatmap of ASE for genes with svASE.

Figure 1—Figure supplement 5. Genes identified as maternally deposited in our data but as zygotically expressed in *Lott et al. (2011)*

Figure 1—Figure supplement 6. Genes identified as zygotically expressed in both crosses in our data but maternally deposited in *Lott et al. (2011)*.

Figure 1—Figure supplement 7. Genes with species-specific expression, regardless of parent of origin

Figure 1—Figure supplement 8. Genes with spatially varying splicing.

87 Consistent with previous observations (*Wittkopp et al., 2006; Coolon et al., 2012*), we did not
88 find any convincing evidence of imprinting (i.e. zygotic transcription of the maternal or paternal copy
89 of a gene). Although we identified 2,778 genes with a strong maternal expression pattern, defined
90 here as 65% of the slices in all embryos having at least 66.7% of transcripts coming from the mother's
91 species, these are consistent with the transcripts having been deposited in the egg. Furthermore
92 no genes expressing primarily maternal transcripts had distinct non-uniform expression, consistent
93 with maternal deposition. We also searched for paternally expressed alleles, which would represent
94 strong evidence of imprinting. Because the two-thirds cutoff was quite conservative, we performed
95 separate t-tests on the ASE values in hybrid embryos with *D. melanogaster* mothers and hybrid
96 embryos with *D. simulans* mothers, and took the larger one-sided p-value (reflecting the significance
97 of paternal bias) for each gene. No genes had even a nominal p-value less than 0.1 (i.e. without
98 correcting for multiple testing), suggesting that there are no paternally-biased genes at this stage of
99 development.

100 Our list of maternally deposited genes is highly concordant with previous measurements of
101 maternal expression. Of the genes classified as maternally expressed in the early expression
102 time-course in *Lott et al. (2011)*, we measured allele-specific expression for 2,653, and found
103 that we clearly agreed on 1,670 (in 552 of the remaining genes, we found the expression to
104 be maternally biased in one of the directions of the cross, but we also detect non-trivial zygotic
105 expression in the other direction). There were also 1,771 maternally provided genes that had low
106 expression (less than 10 FPKM in 65% or more of the slices) in our data, which is consistent with
107 many maternally provided genes being heavily degraded by this point in development. Furthermore,
108 of the 8 genes that *Lott et al. (2011)* classified as zygotically expressed, we classified as maternally
109 expressed, and which had published *in situ* hybridization data, *Tomancak et al. (2002)* detected
110 maternally deposited RNA for 5/8, suggesting that they may be dependent on the precise strain or
111 conditions (*Figure 1*—Figure supplement 4). The 564 genes we classified as not biased that *Lott*
112 *et al. (2011)* classified as maternal are generally weakly biased as maternal, but not enough to clear
113 our thresholds (*Figure 1*—Figure supplement 5).

114 We then looked for genes that are consistently biased towards one species, regardless of parent.
115 We found 572 genes (at a 10% FDR) where the overall expression was more biased than expected
116 by chance (see Methods). However, many of these showed only a weak bias (some cases have as
117 few as 2% more reads from one species than from the other), so we further identified a subset of
118 these with at least 2-fold more reads from one species than the other in 65% of slices; we called
119 this subset strongly biased (see Methods). We found 42 genes with strongly *D. melanogaster*-biased
120 expression, and 38 genes with strongly *D. simulans*-biased expression (*Figure 1*—Figure supplement
121 7). Given that the gene models we are using are taken entirely from *D. melanogaster*, we may
122 be underestimating the true quantity of *D. simulans* biased genes (this caveat does not apply to
123 spatially varying ASE, since inaccurate gene models would not lead to spatial variation across the
124 embryo). Intriguingly, a few of these genes are expressed at comparable levels and with similar
125 spatial patterns in the *D. melanogaster* and *D. simulans* parental embryos, indicating they may be
126 affected by compensatory cis- and trans-acting changes. These species-biased genes are spread
127 throughout the genome, suggesting that this effect is not a consequence of a single cis-regulatory
128 change or inactivation of an entire chromosome.

129 **Spatially varying allele-specific expression highlights genes with cis-regulatory changes**

130 The greatest power of this dataset lies in its ability to identify genes with spatially varying ASE
131 (svASE)—that is, expression in one part of the embryo that is differently biased than another part of
132 the embryo. In order to identify these genes, we fit two different simple patterns to the ASE as a
133 function of embryo position (*Figure 1A*). We identified 40 genes where a sigmoid function explained
134 at least 45% of the variance in ASE (*Figure 1B*), and 21 where a Gaussian function explained at
135 least that much of the variance (*Figure 1C*; if both explained over half the variance for a gene, we
136 only count the one that better explains the variance). In order to estimate a false discovery rate,

137 we shuffled the x -coordinates of the ASE values, and refit the functions. Of 1000 shuffles, only 6
138 (sigmoid) and 0 (peak) genes cleared the threshold for svASE, which implies false discovery rates of
139 $\approx 0.020396\%$ (sigmoid) and $< 0.001925\%$ (peak). At a more relaxed 10% FDR cutoff, we found 320
140 genes where fitting explains at least 12% of the variance in ASE.

141 We observed very few spatially varying splicing differences in our data (**Figure 1**—Figure supple-
142 ment 8). In one case, our data suggest that the shorter *A* isoform of the *kni* gene is preferentially
143 expressed in the posterior expression domain; to our knowledge, spatially varying splicing has not
144 been previously observed for *kni*, though the two expression domains are known to be driven by
145 different trans-regulatory factors (**Rothe et al., 1994**). Most examples of spatially varying splice-
146 junction usage qualitatively matched the svASE for the same gene, though it was noisier due to the
147 smaller number of reads supporting splice junction usage compared to expression. An exception
148 to this involved the maternal-zygotic gene *HnRNP-K*, where the shortest isoform was zygotically
149 expressed, consistent with our previous observations that zygotic transcripts are often short in
150 this stage of *Drosophila* development (**Artieri and Fraser, 2014**). The use of alternative first exons
151 in both of these cases suggests that cis-regulation may contribute to the preponderance of short
152 transcripts during early development, in addition to temporal constraints on the transcription of
153 long genes.

154 Searching for Gene Ontology (GO) function terms enriched for genes with svASE (**Eden et al.,**
155 **2007, 2009**), we found enrichments for genes involved in embryonic morphogenesis (GO:0048598, q -
156 value 2.3×10^{-6}), including transcription factors (GO:0003700, q -value 9.8×10^{-7}) and transmembrane
157 receptors (GO:0099600, q -value 2.2×10^{-2}). These included key components in important signaling
158 pathways, such as *fz2* (a Wnt receptor) and *sog* (a repressor of the TGF- β signaling pathway). *Myc*, a
159 cell cycle regulator that is a target of both of these pathways, also had significant svASE. However,
160 when we used all non-uniformly expressed genes from **Combs and Eisen (2013)** as a background
161 set, we did not find any enriched GO terms, suggesting that the enrichments are driven by functions
162 shared by spatially patterned genes overall, rather than among svASE genes specifically.

163 **A single SNP is the source of svASE in the gap gene *hunchback***

164 We noticed that *hunchback*, an important transcriptional regulator (**Small et al., 1991; Wimmer**
165 **et al., 2000; Jaeger, 2011**), had strong svASE (step-like fit $r^2 = 0.57$; **Figure 1B**). Since the regulation of
166 *hb* is relatively well-characterized, this provided the opportunity to study the sequence-level causes
167 of the svASE that we observed.

168 The *hb* svASE was driven by the anterior tip, which had a strong bias towards the *D. melanogaster*
169 allele, suggesting an expansion of the anterior domain relative to *D. simulans* (**Figure 2A**). Compared
170 to ASE elsewhere in the embryo, ASE in the anterior tip was both stronger (~ 10 -fold more *D.*
171 *melanogaster* transcripts than *D. simulans*), and also less affected by the species of the mother
172 (excluding the first six anterior slices, there are 5-15% more reads from the maternal species than
173 the paternal). When we performed *in situ* hybridization for *hb* RNA, we found overall similar patterns
174 of localization, except in the anterior tip, where we observed *hb* expression in *D. melanogaster*, but
175 not in *D. simulans* (Fig. 2B and C). Although the parental embryos are not precisely the same size,
176 the *in situs* are consistent with the svASE, suggesting that the divergence is not due to embryo size
177 or trans-regulatory changes.

178 We next examined known regulatory sequences near *hb* for changes in TF binding sites that
179 might cause the strong ASE in the anterior tip of the embryo. We downloaded from RedFly all
180 known CRMs and reporter constructs with *hb* as a target (**Gallo et al., 2011**). There are three known
181 minimal CRMs for *hb* that have been tested for embryonic activity using transgenic constructs: the
182 canonical anterior CRM proximal to the *hb* promoter (**Driever and Nüsslein-Volhard, 1989; Schröder**
183 **et al., 1988**), a more distal “shadow” CRM (**Perry et al., 2011**), and an upstream CRM that drives
184 expression in both the anterior and posterior domains, but not the anterior tip of *D. melanogaster*
185 (**Margolis et al., 1995**) (**Figure 3A**). We excluded the upstream CRM from further consideration and
186 used FIMO to scan the other regulatory sequences for motifs of the 14 TFs with CHIP signal near

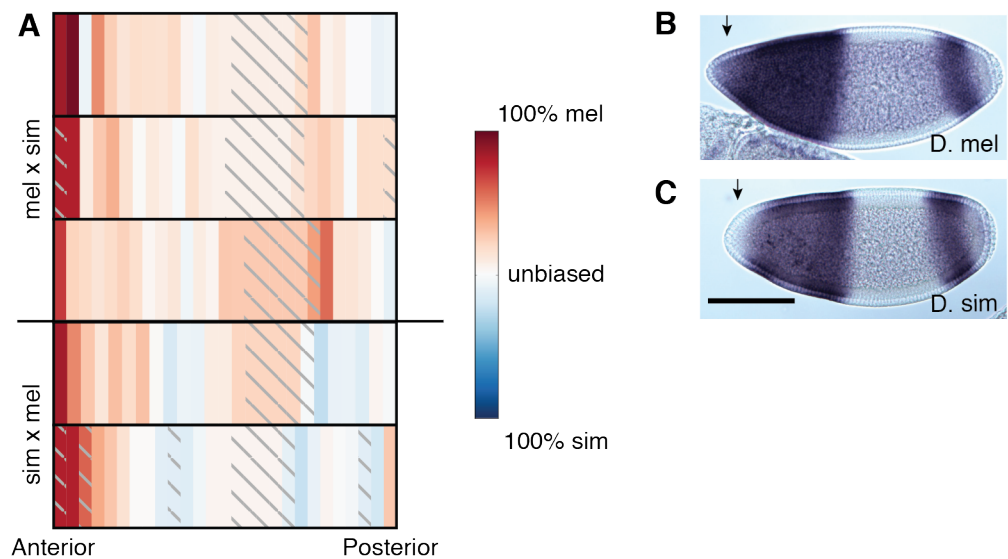


Figure 2. Hybrid embryos show strong melanogaster-specific expression of *hunchback* in the anterior.
A) Heatmap of svASE of *hb* shows a significant *D. melanogaster* bias in the anterior tip of the embryo. Each row is a different embryo. Embryos with a melanogaster mother are above the horizontal line. B-C) *In situ* hybridization for *hb* in parental embryos. Images are arranged anterior to the left and dorsal up.

187 *hb* (Li et al., 2008; Bailey et al., 2015). Binding in the canonical Bicoid-dependent anterior element
188 gained only a single weak Bicoid motif in *D. simulans* relative to *D. melanogaster* (Figure 3B), and
189 the distal “shadow” CRM gained Twist and Dichaete binding motifs between *D. melanogaster* and
190 *D. simulans* (Driever et al., 1989; Perry et al., 2011) (Figure 3C). Unsurprisingly, binding sites for other
191 TFs outside the core regulatory elements displayed pervasive apparent turnover, with multiple
192 gains and losses between the species (Figure 3–Figure supplement 1) (Lusk and Eisen, 2010; He
193 et al., 2011).

194 Anterior zygotic expression of *hb* is driven primarily by Bicoid, but there are details of the
195 expression pattern at mid-stage 5 that cannot be explained by the relatively simple Bicoid gradient,
196 and the loss of expression at the anterior tip of *D. simulans* cannot be explained by additional
197 Bicoid activation. In order to more fully understand how this pattern might be specified and what
198 the effects of binding site changes could be, we took a modeling-based approach similar to Ilsley
199 et al. (2013). We used the 3-dimensional gene expression atlas from Fowlkes et al. (2008) to test
200 regulators in a logistic model for the anterior *hunchback* expression domain (see Methods). The
201 model included a linear term for every gap gene TF bound in the anterior activator CRM (Li et al.,
202 2008) and a quadratic term for Bicoid to account for recent observations that it may lose its ability
203 to act as an activator at high concentrations (Fu and Ma, 2005; Ilsley et al., 2013). The best fit
204 model (Figure 3—data 1) had the strongest coefficients for the two Bicoid terms, consistent with
205 previous studies examining *hb* output as a simple function of Bcd concentration (Driever et al.,
206 1989; Driever and Nüsslein-Volhard, 1989; Gregor et al., 2007). All the other TFs that bind to the
207 locus are understood to be either repressors or have unclear direction of effect; consistent with
208 this, most of the coefficients for those TFs are negative (Reinitz and Levine, 1990; Ganguly et al.,
209 2005; Small et al., 1991). The exceptions to this are D and Twi which act as weak activators in the
210 model, consistent with observations in the literature of bifunctionality for these TFs (Aleksic et al.,
211 2013; Sandmann et al., 2007).

212 We built this model to determine whether any of the binding site changes between *D. melanogaster*
213 and *D. simulans* could plausibly explain the ASE that we observe in *hb*. Therefore, we did not make
214 any effort to determine the minimal set of TFs that would drive the *hb* pattern, nor did we include a
215 term to model predicted autoregulation (Treisman and Desplan, 1989; Holloway et al., 2011).

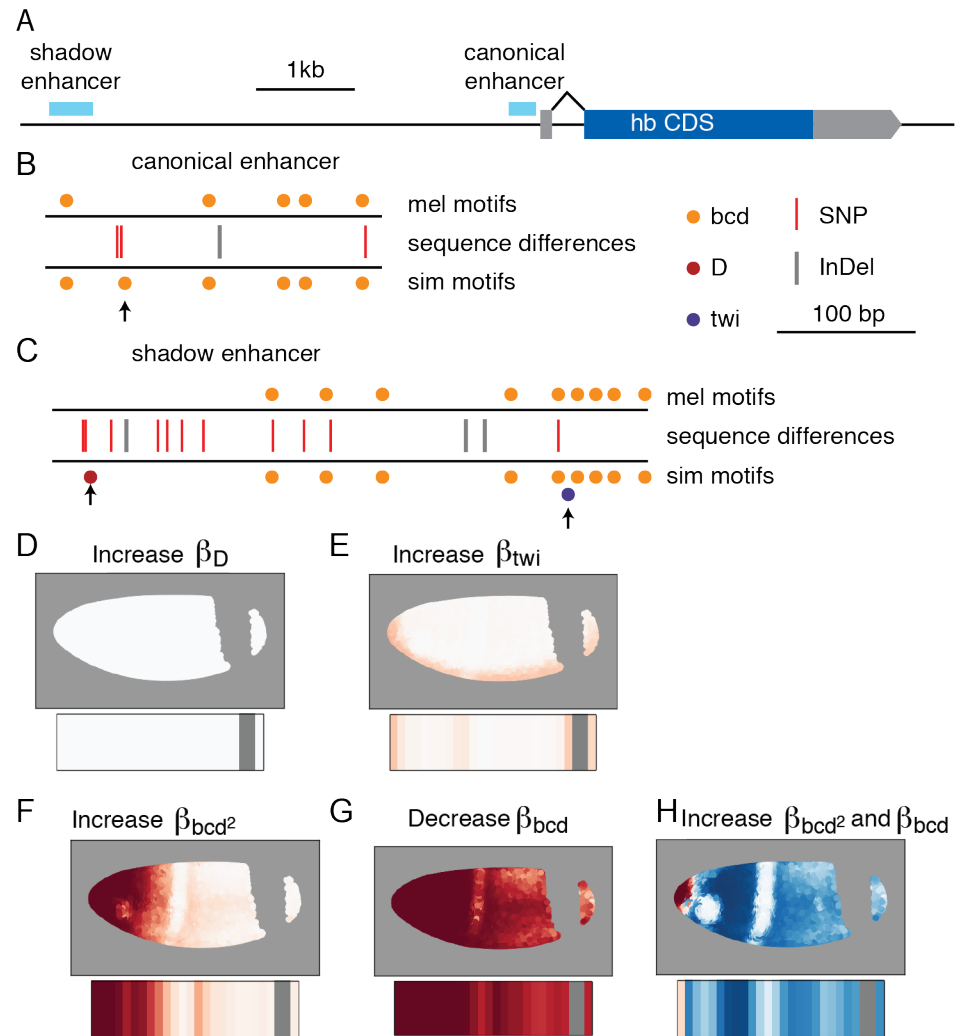


Figure 3. Cis-regulatory changes in *hb* regulatory regions could cause the observed svASE. A) Regulatory elements near the zygotic *hunchback* transcript. B-C) FIMO binding motifs and inter-specific variants of the anterior activator (B) and shadow CRM from *Perry et al. (2011)* (C). Species-specific predicted binding sites are highlighted with arrows. D-H) Predicted ASE from adjusting strength of each TF in the model in order to maximize the variance in the real ASE explained by the predicted ASE. Predicted ASE per nucleus is shown above and predicted ASE in a sliced embryo is shown below.

Figure 3-Figure supplement 1. Motif content of the CRMs for all TFs included in the model.

Figure 3-Figure supplement 2. Coefficients of the best-fit model for TFs bound near the anterior activator of *hb*

Figure 3-Figure supplement 3. Correlation of the predicted *hb* ASE with the real ASE (A) and percent of the variance explained by predicted ASE (B) at a range of coefficient strengths.

Figure 3-Figure supplement 4. Proposed TF binding changes that generate svASE in *Ance*, *bmm*, *CG8147*, and *path*. We did not attempt modeling of the pair-rule genes *pxb*, *Bsg25A*, *comm2*, and *pxb*, since other pair-rule genes have multiple, independent regulatory elements, likely complicating the modeling approach.

216 In order to predict what effect the binding changes would have on expression in a *D. simulans* (or
217 hybrid) embryo, we adjusted the coefficient for each TF independently to find the coefficient that
218 best predicted the observed ASE. We then compared the output of the *D. melanogaster* model to the
219 adjusted one (**Figure 3D-H**). Adjusting the Bcd coefficients, either alone or in tandem, produced the
220 predicted ASE pattern most similar to the actual expression differences we observed between the
221 species. We therefore hypothesized that the additional Bicoid site produced the smaller *D. simulans*
222 *hb* anterior domain.

223 To test this prediction, we used CRISPR-Cas9 and homology-directed repair genome editing
224 to introduce the Bicoid binding site SNPs from *D. simulans* into *D. melanogaster* embryos (**Gratz**
225 **et al., 2014; Port et al., 2014**). In order to avoid any transgene-specific ectopic staining, we edited
226 the endogenous *hunchback* regulatory locus in *D. melanogaster*. We created 2 homozygous lines
227 based on separate integration events, but with identical *D. simulans* sequence at the *hb* regulatory
228 locus. We then tested these lines using *in situ* hybridization, and found that edited lines lose *hb*
229 expression in the anterior tip, making the pattern much more similar to *D. simulans* (**Figure 4** and
230 **Figure 4—Figure supplement 1**).

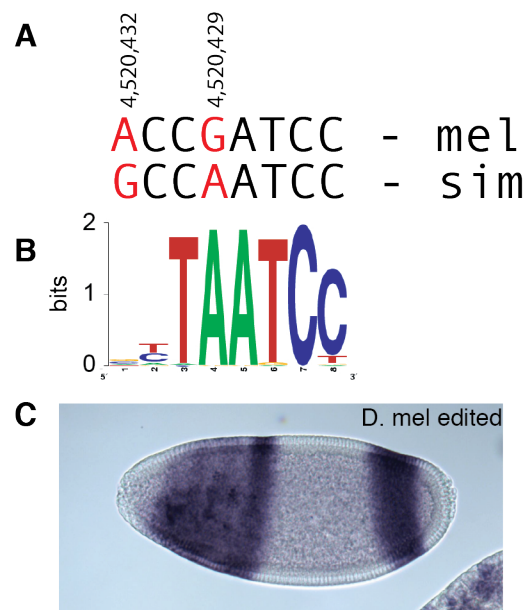


Figure 4. CRISPR-Cas9-mediated editing shows a Bicoid site in *D. simulans* is responsible for the change in expression pattern. A) A pair of SNPs in the canonical *hb* CRM at the indicated coordinates on *D. melanogaster* chromosome 3R. SNPs between *D. melanogaster* and *D. simulans* marked in red. B) The Bicoid binding motif. C) Representative *in situ* hybridization image for *hb* in a *D. melanogaster* embryo with the two base-pairs altered to match the *D. simulans* sequence at the canonical CRM.

Figure 4—Figure supplement 1. A second, independently edited *D. melanogaster* line also shows the anterior gap of hunchback expression

Figure 4—Figure supplement 2. A naturally occurring strain of *D. simulans* with one of the base pair changes found in our edited line does not show the anterior gap of expression, closer to the *D. melanogaster* pattern.

231 We noticed that of the two SNPs that differ between *D. melanogaster* and *D. simulans*, the SNP
232 that is outside of the core Bicoid binding motif is fixed in a survey of 20 *D. simulans* lines, whereas
233 the SNP within the core of the motif (position 4,520,429; **Figure 4A**) is segregating in *D. simulans*
234 and is the minor allele (present in only 3 of the 20 lines in **Rogers et al. (2015)**). To test the role of
235 this variant in isolation, we screened a number of *D. simulans* stocks and found a line, “sim 188”
236 (**Machado et al., 2016**), that had the *D. melanogaster*-like sequence in the core of the Bicoid motif.
237 When we performed *in situ* hybridization, we found that *hunchback* expression was present at the

238 anterior tip of the embryo (**Figure 4**–**Figure supplement 2**), as in *D. melanogaster*, lending further
239 strength to the hypothesis that the difference in expression pattern is due to Bicoid binding, and
240 that the core Bicoid motif SNP is primarily responsible.

241 Discussion

242 The study of allele-specific expression in F1 hybrids is a powerful tool for probing the evolution of
243 gene expression (**Fraser, 2011; Wittkopp and Kalay, 2012**). However, previous studies on *Drosophila*
244 hybrids have been limited in their ability to pinpoint the causal variants responsible for the observed
245 cis-regulatory divergence (**Wittkopp et al., 2004; Graze et al., 2009; Coolon et al., 2014**). In particular,
246 the use of adult samples comprising multiple cell types meant that there was comparatively little
247 information about the regulatory environment. In contrast, by focusing on the *Drosophila* embryo
248 and using spatially-resolved samples, we were able to leverage decades of genetic and functional
249 genomic information in *D. melanogaster* (**Driever and Nüsslein-Volhard, 1989; Tomancak et al.,**
250 **2007; Li et al., 2008; Fowlkes et al., 2008; Gallo et al., 2011; Li et al., 2011; Shazman et al., 2014**).
251 Combining this information with mathematical modeling of gene expression patterns yielded
252 specific, testable predictions about which sequence changes produced the observed expression
253 differences (**Figure 3**). Finally, by using CRISPR-mediated genome editing, we were able to directly
254 confirm the genetic basis of the divergence in *hb* expression.

255 Although we were careful to minimize mapping bias in the detection of ASE, it is possible that
256 non-zero ASE in any given gene is due to purely technical effects. However, by comparing parts
257 of the same embryo to one another, we can effectively control for technical effects; even if the
258 absolute level of ASE is incorrect, the variation is still meaningful. More importantly, changes in
259 the position but not the absolute level of expression would be lost in bulk samples, and spatially
260 restricted expression changes would tend to be washed out by more highly expressed and less
261 variable regions.

262 A previous study found allele-specific expression for ~ 15% of genes in a *D. melanogaster* × *D.*
263 *simulans* hybrid adult (**Coolon et al. (2014)**). Considering that 400-600 genes have AP expression
264 patterns in blastoderm stage embryos (**Tomancak et al., 2007; Combs and Eisen, 2013**), our results
265 suggest a roughly similar fraction of these patterned genes have strong svASE. We chose to restrict
266 our study to the AP axis because it is straightforward to generate well-aligned slices with the long
267 axis of a prolate object; there are no doubt many genes with dorsal-ventral expression differences
268 as well, especially since DV CRMs tend to be shorter (**Li and Wunderlich, 2017**), and thus potentially
269 more sensitive to sequence perturbation than AP CRMs.

270 Our experiment with editing the *hunchback* locus also suggested that Bicoid loses its activator
271 activity at the anterior tip of the embryo. Although **Ilslley et al. (2013)** found that the two Bicoid
272 terms have a net negative effect in the anterior tip of the embryo for *eve*, in our model the balance
273 of the linear activation term and the quadratic repression term is such that at the anterior tip
274 the two approximately cancel each other out. This is consistent with the observations that Torso
275 signaling phosphorylates Bicoid in the anterior and deactivates it (**Ronchi et al., 1993; Janody et al.,**
276 **2000**), rather than making Bicoid function as a transcriptional repressor. On the other hand, despite
277 lacking evidence that Bicoid can act as a repressor, the unmodified shadow CRM (which can drive
278 expression in the anterior tip) is evidently not able to compensate for the reduced activity in the
279 primary *D. simulans* CRM. Nor is it obvious that increased binding of an inactive factor would reduce
280 expression.

281 We were not able to detect any aberrant phenotype of the altered *D. melanogaster* embryos
282 engineered to have the *D. simulans hunchback* expression pattern. This is not surprising—although
283 there are a number of subtle morphological, behavior, and physiological differences between *D.*
284 *melanogaster* and *D. simulans* (**Orgogozo and Stern, 2009**), they are nevertheless generally regarded
285 as indistinguishable as adults (**McNamee and Dytham, 1993**). Development is robust to large
286 variation in the amount of *hunchback*, with hemizygous embryos giving rise to phenotypically normal
287 adults (**Yu and Small, 2008**). Similarly, although embryos with varying Bicoid concentrations have

288 widespread transcriptional changes, development is able to buffer these changes, at least in part
289 due to differential apoptosis at later stages (*Driever and Nüsslein-Volhard, 1988; Liu et al., 2013;*
290 *Combs and Eisen, 2017; Namba et al., 1997*). It is also possible that the reduced *hb* expression in *D.*
291 *simulans* matters only in particular stress conditions, but given the similar cosmopolitan geographic
292 distributions of *D. melanogaster* and *D. simulans*, it is not obvious what conditions those might be.

293 We believe that the informed modeling approach we have taken can serve as a model for
294 dissecting other cis-regulatory modules. Eight genes with clear svASE are present in the BDTNP
295 expression atlas (*Fowlkes et al., 2008*), and preliminary modeling of the four genes without pair-
296 rule-like striping patterns suggested plausible binding site changes that could be responsible
297 (**Figure 3**—Figure supplement 4). In some of these cases, there are multiple binding site changes that
298 could explain our observed svASE equally well, but predict different dorso-ventral gene expression
299 patterns in *D. simulans*—in these cases, *in situ* hybridization for the gene with svASE should provide
300 clearer hypotheses of the causal variants. This approach, when applied more broadly and in concert
301 with evolutionary studies, should help refine our understanding of both the molecular mechanisms
302 and phenotypic consequences of the evolution of spatial patterning.

303 **Materials and Methods**

304 **Strains and hybrid generation**

305 Unless otherwise indicated, we used DGRP-340 as the *D. melanogaster* strain, and w501 as the *D.*
306 *simulans* strain. Males of both species were co-housed for 5 days at 18C in order to improve mating
307 efficiency, then approximately twenty males were mated with ten 0–1 day old virgin females of the
308 opposite species per vial with the stopper pressed almost to the bottom. After cohousing, males
309 were sorted using eye color as a primary marker. 5 days later, flies from the vials with larvae were
310 put into a miniature embryo collection cage with grape juice-agar plates and yeast paste (Genessee
311 Scientific).

312 **RNA extraction, library preparation, and sequencing**

313 We selected single embryos at the target stage (based on depth of membrane invagination) on
314 a Zeiss Axioskop with a QImaging Retiga 6000 camera and transferred them to ethanol-cleaned
315 Peel-a-way cryoslicing molds (Thermo Fisher). We then applied approximately 0.5 μ L of methanol
316 saturated with bromophenol blue (Fisher Biotech, Fair Lawn N.J.), then washed with clean methanol
317 to remove the excess dye. Next, we covered the embryo in Tissue-Plus O.C.T Compound (Fisher
318 Healthcare) and froze the embryo at -80 until slicing. We sliced the embryos using a Microm HM550
319 cryostat, with a fresh blade for each embryo to minimize contamination.

320 We used 1mL of TRIzol (Ambion) with 400 μ g/mL of Glycogen (VWR) to extract RNA, ensuring
321 that the flake of freezing medium was completely dissolved in the TRIzol. In order to determine
322 the sex of each embryo, we generated cDNA from the RNA using SuperScript II (Invitrogen) and a
323 gene-specific primer for *Roc1a*, which is on the X chromosome and has a 49bp *D. simulans* specific
324 insertion. We then amplified bands (Primers: cca gat gga ggg agc agc ac(forward) and atc gcc cca cta
325 gct taa gat ct (reverse) amplicon lengths: 99bp and 138 bp) to determine the sex of hybrid embryos.

326 Next, we randomized the order of the RNA samples (see Supplementary file 1), then prepared
327 libraries using a slightly modified version of the SMART-seq2 protocol (*Picelli et al., 2014*). As
328 described in *Combs and Eisen (2015)*, instead of steps 2-5 of the protocol in *Picelli et al. (2014)*, we
329 added 1 μ L of oligo-dT and 3.7 μ L of dNTP mix per 10 μ L of purified RNA; in step 14, we reduced the
330 pre-amplification to 10 cycles; from step 28 onwards, we reduced the volume of all reagents by
331 five-fold; and at step 33, we used 11 PCR amplification cycles.

332 We sequenced libraries in 4 separate lanes on either an Illumina HiSeq 4000 or an Illumina
333 NextSeq (See Supplementary file 1 for lane and index details).

334 **Sequencing data processing and ASE calling**

335 In order to call mappable SNPs between the species, we used Bowtie 2 (*Langmead and Salzberg,*
336 **2012**, version 2.2.5, arguments `-very-sensitive`) to map previously published genomic sequenc-
337 ing data for the lines in this study (SRR835939, SRR520334 from *Mackay et al., 2012; Hu et al.,*
338 **2013**) onto the FlyBase R5.57 genome. We then used GATK (*DePristo et al., 2011*, version 3.4-
339 46, arguments `-T HaplotypeCaller -genotyping_mode DISCOVERY -output_mode EMIT_ALL_SITES`
340 `-stand_emit_conf 10 -stand_call_conf 30`) to call SNPs.

341 Next, we created a version of the *D. melanogaster* genome with all SNPs that are different
342 between the two species masked. We used STAR (*Dobin et al., 2013*, version 2.4.2a, arguments
343 `-clip5pNbases 6`) to map each sliced RNA-seq sample to the masked genome. We further filtered
344 our list of SNPs to those for which, across all the RNA-seq samples, there were at least 10 reads
345 that supported each allele. We also implemented a filtering step for reads that did not remap to
346 the same location upon computationally reassigning each SNP in a read to the other parent as
347 described in *van de Geijn et al. (2015)*.

348 To call ASE for each sample, we used the GetGeneASEbyReads script in the ASER package
349 (Manuscript in preparation, available at <https://github.com/TheFraserLab/ASER/>, commit cfe619c69).
350 Briefly, each read is assigned to the genome whose SNP alleles it matches. Reads are discarded as
351 ambiguous if there are no SNPs, if there are alleles from both parents, or if the allele at a SNP does
352 not match either parent. Additionally, for most subsequent analyses, ASE is ignored if the gene is
353 on the X chromosome and the slice came from a male embryo (which only have an X chromosome
354 from their mother). All other analysis scripts are available at [https://github.com/TheFraserLab/](https://github.com/TheFraserLab/HybridSliceSeq)
355 *HybridSliceSeq* (commit c244b87).

356 **Earth Mover Distance and Spatial Patterning Differences**

357 Earth mover distance (EMD), as described in *Rubner et al. (1998)*, is a non-parametric metric that
358 compares two distributions of data in a way that roughly captures intuitive notions of similarity. It
359 represents the minimal amount of work (defined as the amount moved multiplied by the distance
360 carried) that must be done to make one pattern equivalent to another, as if transporting dirt
361 from one pile to another. For each slice, we calculate the absolute expression of each gene using
362 cufflinks v.2.2.1 (*Trapnell et al., 2013*). We normalize all absolute expression patterns by first adding
363 a constant amount to mitigate noise in lowly expressed genes, and then by dividing by the total
364 amount of expression in an embryo.

365 To compare between the hybrids and the parental embryos, we first calculated a spline fit for
366 each gene on each of the parental embryos separately, first smoothing by taking a rolling average
367 of 3 slices. We then fit a univariate spline onto the smoothed data using the Scipy “interpolate”
368 package. Then, we recalculated the predicted expression for a hypothetical 27-slice embryo of each
369 parent, then averaged the expression data. We next calculated the EMD between this simulated
370 averaged embryo and each of the hybrid embryos. For each gene, we then performed a one-sided
371 t-test to determine whether the hybrid embryos were more different from the average than the
372 EMD between the parental embryos. Although 342 genes had a nominal p-value < .05, none of
373 these remained significant after Benjamini-Hochberg multiple hypothesis testing correction.

374 To compare embryos between directions of the cross, we calculated the pairwise EMD between
375 embryos within a direction of a cross (i.e. the three possible pairs of hybrid embryos with a
376 *D. melanogaster* mother and the pair of embryos with the *D. simulans* mother) and the pairwise
377 EMD between hybrid embryos with different parents (e.g. the first replicate of embryos). We
378 then used a one-sided t-test to determine whether the EMDs were larger between groups than
379 within. Benjamini-Hochberg FDR estimation yielded 171 genes with a q-value less than .05, whereas
380 Bonferroni p-value correction yielded 12 genes at $\alpha < .05$.

381 **Identification of allele-specific expression patterns**

382 In order to call a gene as strongly biased, we required that gene have at least 10 slices with
383 detectable ASE, with at least 65% of those slices having at least 66.7% of reads from the same
384 parent (maternal, *D. simulans*, or *D. melanogaster*, as appropriate). To detect genes with more subtle,
385 yet consistent, overall ASE we summed the ASE scores for each embryo separately. To create a
386 null distribution, we randomly flipped the sign of each ASE score then summed the ASE of the
387 randomized matrix, repeating 50,000 times. We then combined the p-values from each embryo
388 using Fisher's method, ignoring scores from X-chromosomal genes in male embryos. To estimate
389 a false discovery rate, we compared the number of genes with a given p-value to the number
390 expected at that p-value under a uniform distribution.

391 To call svASE, we fit a 4-variable least-squares regression of either a sigmoidal logistic function
392 ($f(x) = A/(1 + \exp(w(x - x_0))) - y_0$) or a peak-like Gaussian function ($f(x) = A \cdot \exp(-(x - x_0)^2/w^2) - y_0$).
393 We then considered any gene where the fit explained at least 45% of the variance ($R^2 = \sum(A_i -$
394 $f(x_i))^2 / \sum(A_i - \bar{A})^2$, where A_i is the ASE value in the i th slice, and \bar{A} is the average ASE value for that
395 gene) as having svASE.

396 To calculate a false discovery rate, we shuffled the columns (i.e. the spatial coordinates) of the
397 ASE matrix 1,000 times. For each of the shuffles, we fit both of the ASE functions. Most of the
398 shuffled matrices yielded no fits that explained at least 45% of the variance, only a handful of the
399 matrices yielded a single gene that cleared the threshold, and no shuffled matrix had two or more
400 genes that cleared the threshold.

401 **Spatially varying splicing differences**

402 To look for overall spatially varying splicing differences, we used the DEX-seq script `prepare_annotation`
403 to identify exonic parts (Anders et al., 2012). For each exonic part in each slice, we calculated per-
404 cent spliced in (PSI) (Schafer et al., 2015). Then we followed the same fitting procedure as for the
405 allele-specific expression, with the same cutoff of 45% of the variance explained by the fit.

406 To look for spatially varying, allele-specific splicing, we adapted the ideas of Li et al. (2016) to look
407 specifically at reads that support a splice junction. We used the LeafCutter script `leafcutter_cluster`
408 on all of the mapped, de-duplicated reads to identify splice junctions that have at least 50 reads
409 across our entire dataset. Then, for each read mapping to each well-supported splice junction,
410 we used a custom script to assign it to either *D. melanogaster* or *D. simulans* as above. We then
411 calculated an allele-specific splicing preference index as in equation 1 above. Finally, we used the
412 same fitting procedure as above, except we used a relaxed cutoff of 25% of the variance explained,
413 since only 1 gene had greater than 45% of its variance explained by a fit.

414 **Identification of binding site changes and predicted effects on hybrid embryos**

415 For *hunchback* we used the coordinates for the regulatory elements as defined in the RedFly
416 database to extract the sequence of each regulatory region from the reference sequence files (Gallo
417 et al., 2011). For the other genes whose regulatory programs we investigated for causal binding
418 changes, we used Bedtools to find any non-exonic DNase accessible region within 15,000 bp of
419 each gene (Quinlan and Hall, 2010; Thomas et al., 2011). We then used BLAST v2.3.0+ to search for
420 the orthologous region in *D. simulans*. We combined motifs from the databases in Shazman et al.
421 (2014); Enuameh et al. (2013); Kulakovskiy et al. (2009); Kulakovskiy and Makeev (2009); Bergman
422 et al. (2005) by taking the most strongly-supported motif for a given TF, then we used the FIMO tool
423 of the MEME suite to search for binding sites for all TFs with known spatial patterns (Grant et al.,
424 2011; Bailey et al., 2015).

425 In order to construct a model of transcription regulation for the other genes with svASE and
426 simple expression patterns in the Fowlkes et al. (2008) atlas, we built models that contained the
427 TFs with binding changes for the target gene as well as up to 4 other TFs with localization data
428 in the Fowlkes et al. (2008) atlas and known roles as patterning factors during early development
429 (i.e. Bcd, Gt, Kr, *cad*, *tll*, *D*, *da*, *dl*, *mad*, *med*, *shn*, *sna*, *twi*, *zen*, *brk*, *emc*, *numb*, *rho*, *tkv* and *Doc2*);

430 when available, we used protein localizations instead of RNA *in situ* hybridization (i.e. for Bcd,
431 Gt, and Kr). For a given combination of factors, we used the Python Statsmodels package to fit a
432 logistic regression to the anterior stripe of *hunchback* (Seabold and Perktold, 2010). In line with the
433 procedure in Ilsley et al. (2013), we separated the two *hunchback* expression domains and fit the
434 data on nuclei with either the anterior stripe or no *hunchback* expression. We then selected the
435 best model based on fraction of variance in the original data explained by the fit.

436 To estimate the likely effect of each transcription factor change, we adjusted the relevant
437 parameter(s) in the model by a range of values (see Figure 3—Figure supplement 3). We then
438 generated predicted svASE by predicting expression in each nucleus under the original model and
439 the model with the relevant parameter(s) changed, grouping the nuclei by x-coordinate to simulate
440 slicing, then combining the expression of each nucleus i in each slice s in an analogous manner to
441 equation 1:

$$ASE_{predicted} = \left(\sum_{i \in s} f_{sim}(i) - \sum_{i \in s} f_{mel}(i) \right) / \left(\sum_{i \in s} f_{sim}(i) + \sum_{i \in s} f_{mel}(i) \right) \quad (2)$$

442 We then computed the Pearson correlation of the predicted and real ASE values and measured the
443 fraction of the variance in the real ASE explained by the predicted ASE. In general, both measurement
444 approaches suggested the same direction of change to the coefficient, although the absolute
445 magnitude of change that yielded the “best” result may have been different.

446 Genome Editing and Screening

447 We inserted the *D. simulans* SNPs into *D. melanogaster* using CRISPR-Cas9 directed cutting followed
448 by homology directed repair (Gratz et al., 2014). We inserted the gRNA sequence GGT ACA GGT
449 CGC GGA TCG GT into pU6-bbsI (a generous gift from Tim Mosca and Liqun Luo). We injected the
450 plasmid and a 133bp ssDNA HDR template (IDT, San Diego, CA) into y[1] Mvas-Cas9ZH2A w[1118]
451 embryos (Bloomington Stock #51323, BestGene Inc, Chino Hills, CA). The edited sequence affects
452 a recognition sequence for the restriction enzymes BsiE1 and MspI (New England Biolabs) which
453 specifically cut the *D. melanogaster* and *D. simulans* sequences, respectively. We screened putatively
454 edited offspring by PCR amplifying a region around the *hunchback* anterior CRM (primers CGT CAA
455 GGG ATT AGA TGG GC and CCC CAT AGA AAA CCG GTG GA) then cutting with each enzyme separately.
456 Presumptively edited lines were then further screened via Sanger sequencing.

457 For the *in situ* hybridization, we generated DIG-labeled antisense RNA probes by first performing
458 RT-PCR on *D. melanogaster hunchback* cDNA using primers with a T7 RNA polymerase handle
459 (AAC ATC CAA AGG ACG AAA CG and TAA TAC GAC TCA CTA TAG GGA GA), then creating full-length
460 probes with 2:1 DIG-labeled UTP to unlabeled UTP (Weiszmann et al., 2009). We then performed *in*
461 *situ* hybridization in 2-4 hour old embryos of each strain according to a minimally modified, low-
462 throughput version of the protocol in Weiszmann et al. (2009) ([https://www.protocols.io/view/in-](https://www.protocols.io/view/in-situ-hybridization-g7bbzin)
463 [situ-hybridization-g7bbzin](https://www.protocols.io/view/in-situ-hybridization-g7bbzin)). Stained embryos were imaged on the Zeiss Axioskop above.

464 Additional Files

465 RNA-seq data is available from the Gene Expression Omnibus with accession [GSE102233](https://www.ncbi.nlm.nih.gov/geo/query/acc.cgi?acc=GSE102233).

466 **Supplementary data file 1** Summary description of library construction and sequencing informa-
467 tion, including Nextera barcodes, sequencer type, and lane.

468 **Supplementary data file 2** Allele-specific expression matrix.

469 Acknowledgements

470 We would like to thank Dmitri Petrov for the generous use of incubators and space for fly work. We
471 thank the entire Fraser lab for discussions and advice.

References

- 472
473 **Aleksic J**, Ferrero E, Fischer B, Shen SP, Russell S. The role of Dichaete in transcriptional regulation during
474 *Drosophila* embryonic development. *BMC Genomics*. 2013 Dec; 14(1):861.
- 475 **Anders S**, Reyes A, Huber W. Detecting differential usage of exons from RNA-seq data. *Genome Research*. 2012
476 Oct; 22(10):2008–2017.
- 477 **Artieri CG**, Fraser HB. Transcript length mediates developmental timing of gene expression across *Drosophila*.
478 *Molecular Biology and Evolution*. 2014 Nov; 31(11):2879–2889.
- 479 **Bailey TL**, Johnson J, Grant CE, Noble WS. The MEME Suite. *Nucleic Acids Research*. 2015 Jul; 43(W1):W39–49.
- 480 **Banerji J**, Rusconi S, Schaffner W. Expression of a beta-globin gene is enhanced by remote SV40 DNA sequences.
481 *Cell*. 1981 Dec; 27(2 Pt 1):299–308.
- 482 **Benjamini Y**, Hochberg Y. Controlling the false discovery rate: a practical and powerful approach to multiple
483 testing. *Journal of the royal statistical society Series B (. . . . 1995; 57(1):289–300.*
- 484 **Bergman CM**, Carlson JW, Celniker SE. *Drosophila* DNase I footprint database: a systematic genome annotation
485 of transcription factor binding sites in the fruitfly, *Drosophila melanogaster*. *Bioinformatics (Oxford, England)*.
486 2005 Apr; 21(8):1747–1749.
- 487 **Berthelot C**, Villar D, Horvath JE, Odom DT, Flicek P. Complexity and conservation of regulatory landscapes
488 underlie evolutionary resilience of mammalian gene expression. *bioRxiv*. 2017 Apr; p. 1–31.
- 489 **Combs PA**. Sequencing mRNA from cryosliced *Drosophila* embryos to screen genome-wide patterning changes.
490 PhD thesis, University of California, Berkeley; 2015.
- 491 **Combs PA**, Eisen MB. Sequencing mRNA from cryo-sliced *Drosophila* embryos to determine genome-wide
492 spatial patterns of gene expression. *PLoS ONE*. 2013; 8(8):e71820.
- 493 **Combs PA**, Eisen MB. Low-cost, low-input RNA-seq protocols perform nearly as well as high-input protocols.
494 *PeerJ*. 2015; 3:e869.
- 495 **Combs PA**, Eisen MB. Genome-wide measurement of spatial expression in patterning mutants of *Drosophila*
496 *melanogaster*. *F1000Research*. 2017 Jan; 6:41–15.
- 497 **Coolon JD**, McManus CJ, Stevenson KR, Graveley BR, Wittkopp PJ. Tempo and mode of regulatory evolution in
498 *Drosophila*. *Genome Research*. 2014 May; 24(5):797–808.
- 499 **Coolon JD**, Stevenson KR, McManus CJ, Graveley BR, Wittkopp PJ. Genomic imprinting absent in *Drosophila*
500 *melanogaster* adult females. *Cell reports*. 2012 Jul; 2(1):69–75.
- 501 **DePristo MA**, Banks E, Poplin R, Garimella KV, Maguire JR, Hartl C, Philippakis AA, del Angel G, Rivas MA, Hanna
502 M, McKenna A, Fennell TJ, Kernytsky AM, Sivachenko AY, Cibulskis K, Gabriel SB, Altshuler D, Daly MJ. A
503 framework for variation discovery and genotyping using next-generation DNA sequencing data. *Nature*
504 *Genetics*. 2011 May; 43(5):491–498.
- 505 **DoBin A**, Davis CA, Schlesinger F, Drenkow J, Zaleski C, Jha S, Batut P, Chaisson M, Gingeras TR. STAR: ultrafast
506 universal RNA-seq aligner. *Bioinformatics (Oxford, England)*. 2013 Jan; 29(1):15–21.
- 507 **Driever W**, Nüsslein-Volhard C. The bicoid protein determines position in the *Drosophila* embryo in a
508 concentration-dependent manner. *Cell*. 1988 Jul; 54(1):95–104.
- 509 **Driever W**, Nüsslein-Volhard C. The bicoid protein is a positive regulator of hunchback transcription in the early
510 *Drosophila* embryo. *Nature*. 1989 Jan; 337(6203):138–143.
- 511 **Driever W**, Thoma G, Nüsslein-Volhard C. Determination of spatial domains of zygotic gene expression in the
512 *Drosophila* embryo by the affinity of binding sites for the bicoid morphogen. *Nature*. 1989 Aug; 340(6232):363–
513 367.
- 514 **Eden E**, Lipson D, Yogev S, Yakhini Z. Discovering motifs in ranked lists of DNA sequences. *PLoS Computational*
515 *Biology*. 2007 Mar; 3(3):e39.
- 516 **Eden E**, Navon R, Steinfeld I, Lipson D, Yakhini Z. GOrilla: a tool for discovery and visualization of enriched GO
517 terms in ranked gene lists. *BMC bioinformatics*. 2009 Feb; 10:48.

- 518 **Enuameh MS**, Asriyan Y, Richards A, Christensen RG, Hall VL, Kazemian M, Zhu C, Pham H, Cheng Q, Blatti CA,
519 Brasefield JA, Basciotta MD, Ou J, McNulty JC, Zhu LJ, Celniker SE, Sinha S, Stormo GD, Brodsky MH, Wolfe SA.
520 Global analysis of *Drosophila* Cys2-His2 zinc finger proteins reveals a multitude of novel recognition motifs
521 and binding determinants. *Genome Research*. 2013 Jun; 23(6):928–940.
- 522 **Ferree PM**, Barbash DA. Species-specific heterochromatin prevents mitotic chromosome segregation to cause
523 hybrid lethality in *Drosophila*. *PLoS Biology*. 2009 Oct; 7(10):e1000234.
- 524 **Fowlkes CC**, Hendriks CLL, Keränen SVE, Weber GH, Rübél O, Huang MY, Chatoor S, DePace AH, Simirenko
525 L, Henriquez C, Beaton A, Weiszmann R, Celniker S, Hamann B, Knowles DW, Biggin MD, Eisen MB, Malik
526 J. A quantitative spatiotemporal atlas of gene expression in the *Drosophila* blastoderm. *Cell*. 2008 Apr;
527 133(2):364–374.
- 528 **Fraser HB**. Genome-wide approaches to the study of adaptive gene expression evolution. *BioEssays*. 2011 Apr;
529 33(6):469–477.
- 530 **Fu D**, Ma J. Interplay between positive and negative activities that influence the role of Bicoid in transcription.
531 *Nucleic Acids Research*. 2005; 33(13):3985–3993.
- 532 **Gallo SM**, Gerrard DT, Miner D, Simich M, Des Soye B, Bergman CM, Halfon MS. REDfly v3.0: toward a compre-
533 hensive database of transcriptional regulatory elements in *Drosophila*. *Nucleic Acids Research*. 2011 Jan;
534 39(Database issue):D118–23.
- 535 **Ganguly A**, Jiang J, Ip YT. *Drosophila* WntD is a target and an inhibitor of the Dorsal/Twist/Snail network in the
536 gastrulating embryo. *Development*. 2005 Aug; 132(15):3419–3429.
- 537 **van de Geijn B**, McVicker G, Gilad Y, Pritchard JK. WASP: allele-specific software for robust molecular quantitative
538 trait locus discovery. *Nature Methods*. 2015 Nov; 12(11):1061–1063.
- 539 **Grant CE**, Bailey TL, Noble WS. FIMO: scanning for occurrences of a given motif. *Bioinformatics (Oxford,*
540 *England)*. 2011 Apr; 27(7):1017–1018.
- 541 **Gratz SJ**, Ukken FP, Rubinstein CD, Thiede G, Donohue LK, Cummings AM, O'Connor-Giles KM. Highly specific and
542 efficient CRISPR/Cas9-catalyzed homology-directed repair in *Drosophila*. *Genetics*. 2014 Apr; 196(4):961–971.
- 543 **Graze RM**, McIntyre LM, Main BJ, Wayne ML, Nuzhdin SV. Regulatory divergence in *Drosophila melanogaster*
544 and *D. simulans*, a genomewide analysis of allele-specific expression. *Genetics*. 2009 Oct; 183(2):547–61–
545 1S1–21S1.
- 546 **Gregor T**, Tank DW, Wieschaus EF, Bialek W. Probing the limits to positional information. *Cell*. 2007 Jul;
547 130(1):153–164.
- 548 **He BZ**, Holloway AK, Maerkl SJ, Kreitman M. Does positive selection drive transcription factor binding site
549 turnover? A test with *Drosophila* cis-regulatory modules. *PLoS Genetics*. 2011 Apr; 7(4):e1002053.
- 550 **Holloway DM**, Lopes FJP, da Fontoura Costa L, Travençolo BAN, Golyandina N, Usevich K, Spirov AV. Gene
551 expression noise in spatial patterning: hunchback promoter structure affects noise amplitude and distribution
552 in *Drosophila* segmentation. *PLoS Computational Biology*. 2011; 7(2):e1001069.
- 553 **Hu TT**, Eisen MB, Thornton KR, Andolfatto P. A second-generation assembly of the *Drosophila simulans* genome
554 provides new insights into patterns of lineage-specific divergence. *Genome Research*. 2013 Jan; 23(1):89–98.
- 555 **Ilsley GR**, Fisher J, Apweiler R, DePace AH, Luscombe NM. Cellular resolution models for even skipped regulation
556 in the entire *Drosophila* embryo. *eLife*. 2013; 2:e00522.
- 557 **Jaeger J**. The gap gene network. *Cellular and molecular life sciences : CMLS*. 2011 Jan; 68(2):243–274.
- 558 **Janody F**, Sturny R, Catala F, Desplan C, Dostatni N. Phosphorylation of bicoid on MAP-kinase sites: contribution
559 to its interaction with the torso pathway. *Development*. 2000 Jan; 127(2):279–289.
- 560 **Kulakovskiy IV**, Makeev VJ. Discovery of DNA motifs recognized by transcription factors through integration of
561 different experimental sources. *Biophysics*. 2009; 54(6):667–674.
- 562 **Kulakovskiy IV**, Favorov AV, Makeev VJ. Motif discovery and motif finding from genome-mapped DNase
563 footprint data. *Bioinformatics (Oxford, England)*. 2009 Sep; 25(18):2318–2325.
- 564 **Langmead B**, Salzberg SL. Fast gapped-read alignment with Bowtie 2. *Nature Methods*. 2012 Apr; 9(4):357–359.

- 565 **Li L**, Wunderlich ZB. An Enhancer's Length and Composition Are Shaped by Its Regulatory Task. *Frontiers in*
566 *genetics*. 2017; 8:63.
- 567 **Li Xy**, MacArthur S, Bourgon R, Nix D, Pollard DA, Iyer VN, Hechmer A, Simirenko L, Stapleton M, Luengo Hendriks
568 CL, Chu HC, Ogawa N, Inwood W, Sementchenko V, Beaton A, Weiszmann R, Celniker SE, Knowles DW, Gingeras
569 T, Speed TP, et al. Transcription factors bind thousands of active and inactive regions in the *Drosophila*
570 blastoderm. *PLoS Biology*. 2008 Feb; 6(2):e27.
- 571 **Li Xy**, Thomas S, Sabo PJ, Eisen MB, Stamatoyannopoulos JA, Biggin MD. The role of chromatin accessibility in
572 directing the widespread, overlapping patterns of *Drosophila* transcription factor binding. *Genome Biology*.
573 2011; 12(4):R34.
- 574 **Li Yi**, Knowles DA, Pritchard JK. LeafCutter: Annotation-free quantification of RNA splicing. *bioRxiv*. 2016; .
- 575 **Liu F**, Morrison AH, Gregor T. Dynamic interpretation of maternal inputs by the *Drosophila* segmentation
576 gene network. *Proceedings of the National Academy of Sciences of the United States of America*. 2013 Apr;
577 110(17):6724–6729.
- 578 **Lott SE**, Villalta JE, Schroth GP, Luo S, Tonkin LA, Eisen MB. Noncanonical compensation of zygotic X transcription
579 in early *Drosophila melanogaster* development revealed through single-embryo RNA-seq. *PLoS Biology*. 2011;
580 9(2):e1000590.
- 581 **Ludwig MZ**, Kreitman M. Evolutionary dynamics of the enhancer region of even-skipped in *Drosophila*. *Molecular*
582 *Biology and Evolution*. 1995 Nov; 12(6):1002–1011.
- 583 **Lusk RW**, Eisen MB. Evolutionary mirages: selection on binding site composition creates the illusion of conserved
584 grammars in *Drosophila* enhancers. *PLoS Genetics*. 2010 Jan; 6(1):e1000829.
- 585 **Machado HE**, Bergland AO, O'Brien KR, Behrman EL, Schmidt PS, Petrov DA. Comparative population genomics
586 of latitudinal variation in *Drosophila simulans* and *Drosophila melanogaster*. *Molecular ecology*. 2016 Feb;
587 25(3):723–740.
- 588 **Mackay TFC**, Richards S, Stone EA, Barbadilla A, Ayroles JF, Zhu D, Casillas S, Han Y, Magwire MM, Cridland
589 JM, Richardson MF, Anholt RRH, Barrón M, Bess C, Blankenburg KP, Carbone MA, Castellano D, Chaboub
590 L, Duncan L, Harris Z, et al. The *Drosophila melanogaster* Genetic Reference Panel. *Nature*. 2012 Feb;
591 482(7384):173–178.
- 592 **Margolis JS**, Borowsky ML, Steingrímsson E, Shim CW, Lengyel JA, Posakony JW. Posterior stripe expression
593 of hunchback is driven from two promoters by a common enhancer element. *Development*. 1995 Jul;
594 121(9):3067–3077.
- 595 **McNamee S**, Dytham C. Morphometric discrimination of the sibling species. *Systematic entomology*. 1993; .
- 596 **Namba R**, Pazdera TM, Cerrone RL, Minden JS. *Drosophila* embryonic pattern repair: how embryos respond to
597 bicoid dosage alteration. *Development*. 1997 Apr; 124(7):1393–1403.
- 598 **Orgogozo V**, Stern DL. How different are recently diverged species?: more than 150 phenotypic differences
599 have been reported for the *D. melanogaster* species subgroup. *Fly*. 2009 Apr; 3(2):117.
- 600 **Perry MW**, Boettiger AN, Levine M. Multiple enhancers ensure precision of gap gene-expression patterns in the
601 *Drosophila* embryo. *Proceedings of the National Academy of Sciences of the United States of America*. 2011
602 Aug; 108(33):13570–13575.
- 603 **Picelli S**, Björklund AK, Faridani OR, Sagasser S, Winberg G, Sandberg R. Smart-seq2 for sensitive full-length
604 transcriptome profiling in single cells. *Nature Methods*. 2013 Nov; 10(11):1096–1098.
- 605 **Picelli S**, Faridani OR, Björklund AK, Winberg G, Sagasser S, Sandberg R. Full-length RNA-seq from single cells
606 using Smart-seq2. *Nature Protocols*. 2014 Jan; 9(1):171–181.
- 607 **Port F**, Chen HM, Lee T, Bullock SL. Optimized CRISPR/Cas tools for efficient germline and somatic genome
608 engineering in *Drosophila*. *Proceedings of the National Academy of Sciences of the United States of America*.
609 2014 Jul; 111(29):E2967–76.
- 610 **Ptashne M**. Gene regulation by proteins acting nearby and at a distance. *Nature*. 1986 Aug; 322(6081):697–701.
- 611 **Quinlan AR**, Hall IM. BEDTools: a flexible suite of utilities for comparing genomic features. *Bioinformatics*
612 (Oxford, England). 2010 Mar; 26(6):841–842.

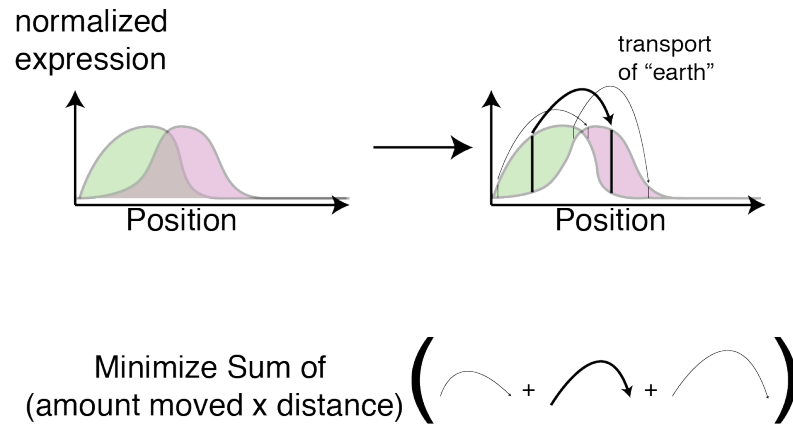
- 613 **Reinitz J**, Levine M. Control of the initiation of homeotic gene expression by the gap genes giant and tailless in
614 *Drosophila*. *Developmental Biology*. 1990 Jul; 140(1):57–72.
- 615 **Rogers RL**, Cridland JM, Shao L, Hu TT, Andolfatto P, Thornton KR. Tandem Duplications and the Limits of Natural
616 Selection in *Drosophila yakuba* and *Drosophila simulans*. *PLoS ONE*. 2015; 10(7):e0132184.
- 617 **Ronchi E**, Treisman J, Dostatni N, Struhl G, Desplan C. Down-regulation of the *Drosophila* morphogen bicoid by
618 the torso receptor-mediated signal transduction cascade. *Cell*. 1993 Jul; 74(2):347–355.
- 619 **Rothe M**, Wimmer EA, Pankratz MJ, Gonzales-Gaitan M, Jäckle H. Identical transacting factor requirement for
620 knirps and knirps-related gene expression in the anterior but not in the posterior region of the *Drosophila*
621 embryo. *Mechanisms of ...* 1994; 46(3):169–181.
- 622 **Rubner Y**, Tomasi C, Guibas LJ. A metric for distributions with applications to image databases. In: *Computer*
623 *Vision, . Sixth International Conference on IEEE*; 1998. p. 59–66.
- 624 **Samee MAH**, Sinha S. Quantitative modeling of a gene's expression from its intergenic sequence. *PLoS*
625 *Computational Biology*. 2014 Mar; 10(3):e1003467.
- 626 **Sandmann T**, Girardot C, Brehme M, Tongprasit W, Stolc V, Furlong EEM. A core transcriptional network for
627 early mesoderm development in *Drosophila melanogaster*. *Genes & Development*. 2007 Feb; 21(4):436–449.
- 628 **Sayal R**, Dresch JM, Pushel I, Taylor BR, Arnosti DN. Quantitative perturbation-based analysis of gene expression
629 predicts enhancer activity in early *Drosophila* embryo. *eLife*. 2016; 5.
- 630 **Schafer S**, Miao K, Benson CC, Heinig M, Cook SA, Hubner N. Alternative Splicing Signatures in RNA-seq Data:
631 Percent Spliced in (PSI). *Current protocols in human genetics*. 2015 Oct; 87:11.16.1–14.
- 632 **Schröder C**, Tautz D, Seifert E, Jäckle H. Differential regulation of the two transcripts from the *Drosophila* gap
633 segmentation gene hunchback. *The EMBO journal*. 1988 Sep; 7(9):2881–2887.
- 634 **Seabold S**, Perktold J. Statsmodels: Econometric and statistical modeling with python. In: *Proceedings of the 9th*
635 *Python in Science ...*; 2010. p. 57–61.
- 636 **Shazman S**, Lee H, Socol Y, Mann RS, Honig B. OnTheFly: a database of *Drosophila melanogaster* transcription
637 factors and their binding sites. *Nucleic Acids Research*. 2014 Jan; 42(Database issue):D167–71.
- 638 **Small S**, Kraut R, Hoey T, Warrior R, Levine M. Transcriptional regulation of a pair-rule stripe in *Drosophila*.
639 *Genes & Development*. 1991 May; 5(5):827–839.
- 640 **Thomas S**, Li Xy, Sabo PJ, Sandstrom R, Thurman RE, Canfield TK, Giste E, Fisher W, Hammonds A, Celniker SE,
641 Biggin MD, Stamatoyannopoulos JA. Dynamic reprogramming of chromatin accessibility during *Drosophila*
642 embryo development. *Genome Biology*. 2011; 12(5):R43.
- 643 **Tomancak P**, Beaton A, Weiszmam R, Kwan E, Shu S, Lewis SE, Richards S, Ashburner M, Hartenstein V, Celniker
644 SE, Rubin GM. Systematic determination of patterns of gene expression during *Drosophila* embryogenesis.
645 *Genome Biology*. 2002; 3(12):RESEARCH0088.
- 646 **Tomancak P**, Berman BP, Beaton A, Weiszmam R, Kwan E, Hartenstein V, Celniker SE, Rubin GM. Global analysis
647 of patterns of gene expression during *Drosophila* embryogenesis. *Genome Biology*. 2007; 8(7):R145.
- 648 **Trapnell C**, Hendrickson DG, Sauvageau M, Goff L, Rinn JL, Pachter L. Differential analysis of gene regulation at
649 transcript resolution with RNA-seq. *Nature Biotechnology*. 2013 Jan; 31(1):46–53.
- 650 **Treisman J**, Desplan C. The products of the *Drosophila* gap genes hunchback and Krüppel bind to the hunchback
651 promoters. *Nature*. 1989 Sep; 341(6240):335–337.
- 652 **Villar D**, Berthelot C, Aldridge S, Rayner TF, Lukk M, Pignatelli M, Park TJ, Deaville R, Erichsen JT, Jasinska AJ,
653 Turner JMA, Bertelsen MF, Murchison EP, Flicek P, Odom DT. Enhancer Evolution across 20 Mammalian Species.
654 *Cell*. 2015 Jan; 160(3):554–566.
- 655 **Weiszmam R**, Hammonds AS, Celniker SE. Determination of gene expression patterns using high-throughput
656 RNA in situ hybridization to whole-mount *Drosophila* embryos. *Nature Protocols*. 2009; 4(5):605–618.
- 657 **Wimmer EA**, Carleton A, Harjes P, Turner T, Desplan C. Bicoid-independent formation of thoracic segments in
658 *Drosophila*. *Science (New York, NY)*. 2000 Mar; 287(5462):2476–2479.

- 659 **Wittkopp PJ**, Haerum BK, Clark AG. Evolutionary changes in cis and trans gene regulation. *Nature*. 2004 Jul;
660 430(6995):85–88.
- 661 **Wittkopp PJ**, Haerum BK, Clark AG. Parent-of-origin effects on mRNA expression in *Drosophila melanogaster*
662 not caused by genomic imprinting. *Genetics*. 2006 Jul; 173(3):1817–1821.
- 663 **Wittkopp PJ**, Kalay G. Cis-regulatory elements: molecular mechanisms and evolutionary processes underlying
664 divergence. *Nature reviews Genetics*. 2012 Jan; 13(1):59–69.
- 665 **Yu D**, Small S. Precise registration of gene expression boundaries by a repressive morphogen in *Drosophila*.
666 *Current biology* : CB. 2008 Jun; 18(12):868–876.

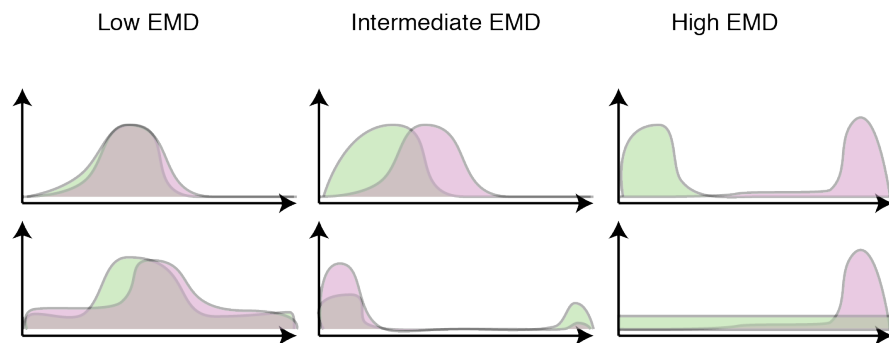
	Mother's species x Father's species	Sex of Embryo	Number of slices
	<i>D. melanogaster</i> x <i>D. melanogaster</i>	Female	27
	<i>D. melanogaster</i> x <i>D. simulans</i>	Female	26
	<i>D. melanogaster</i> x <i>D. simulans</i>	Female	27
667	<i>D. melanogaster</i> x <i>D. simulans</i>	Male	25
	<i>D. simulans</i> x <i>D. melanogaster</i>	Female	27
	<i>D. simulans</i> x <i>D. melanogaster</i>	Male	27
	<i>D. simulans</i> x <i>D. simulans</i>	Male	27

Figure 1-Figure supplement 1. Summary data for embryos used

A

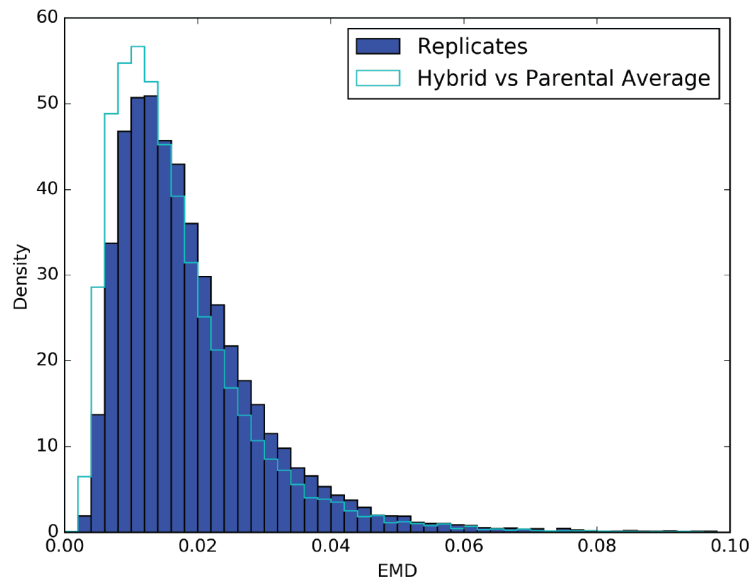


B



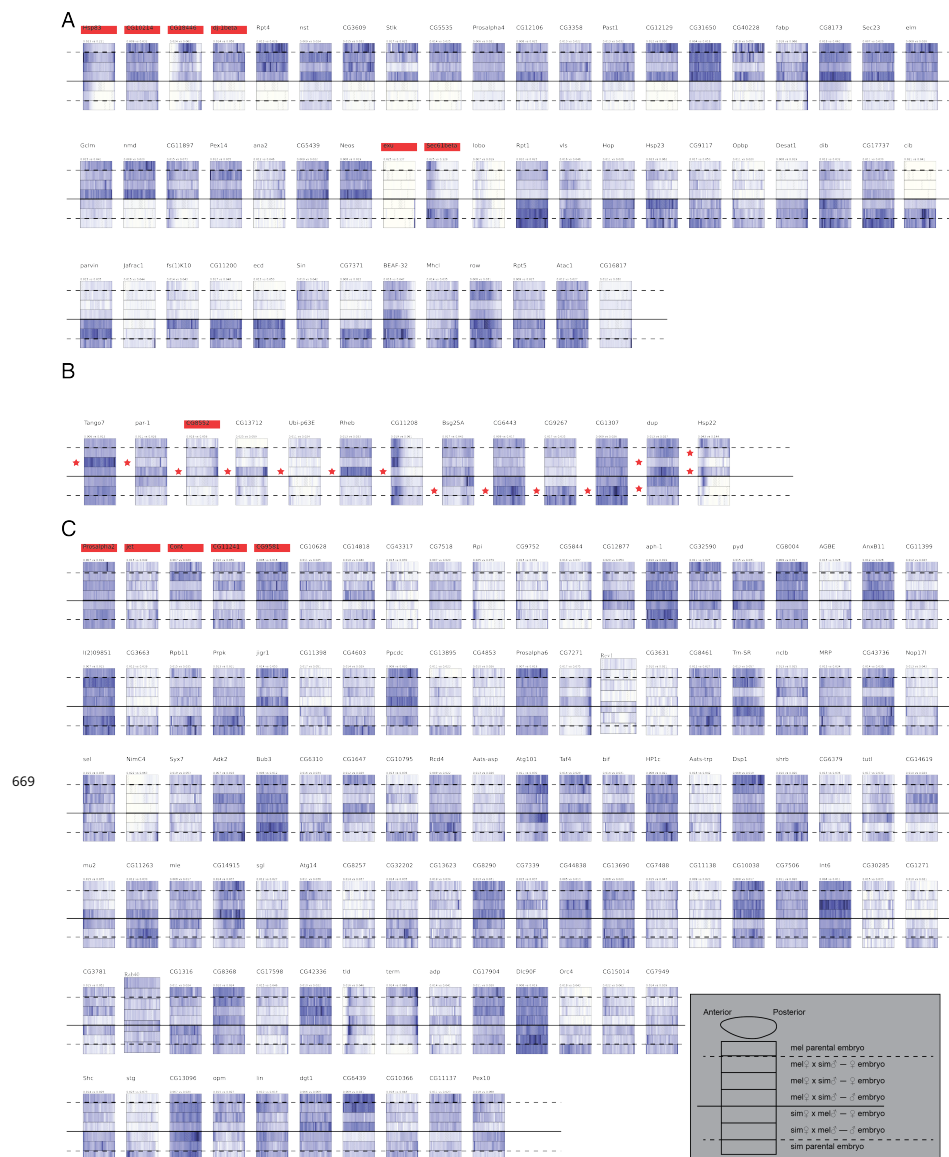
668

C



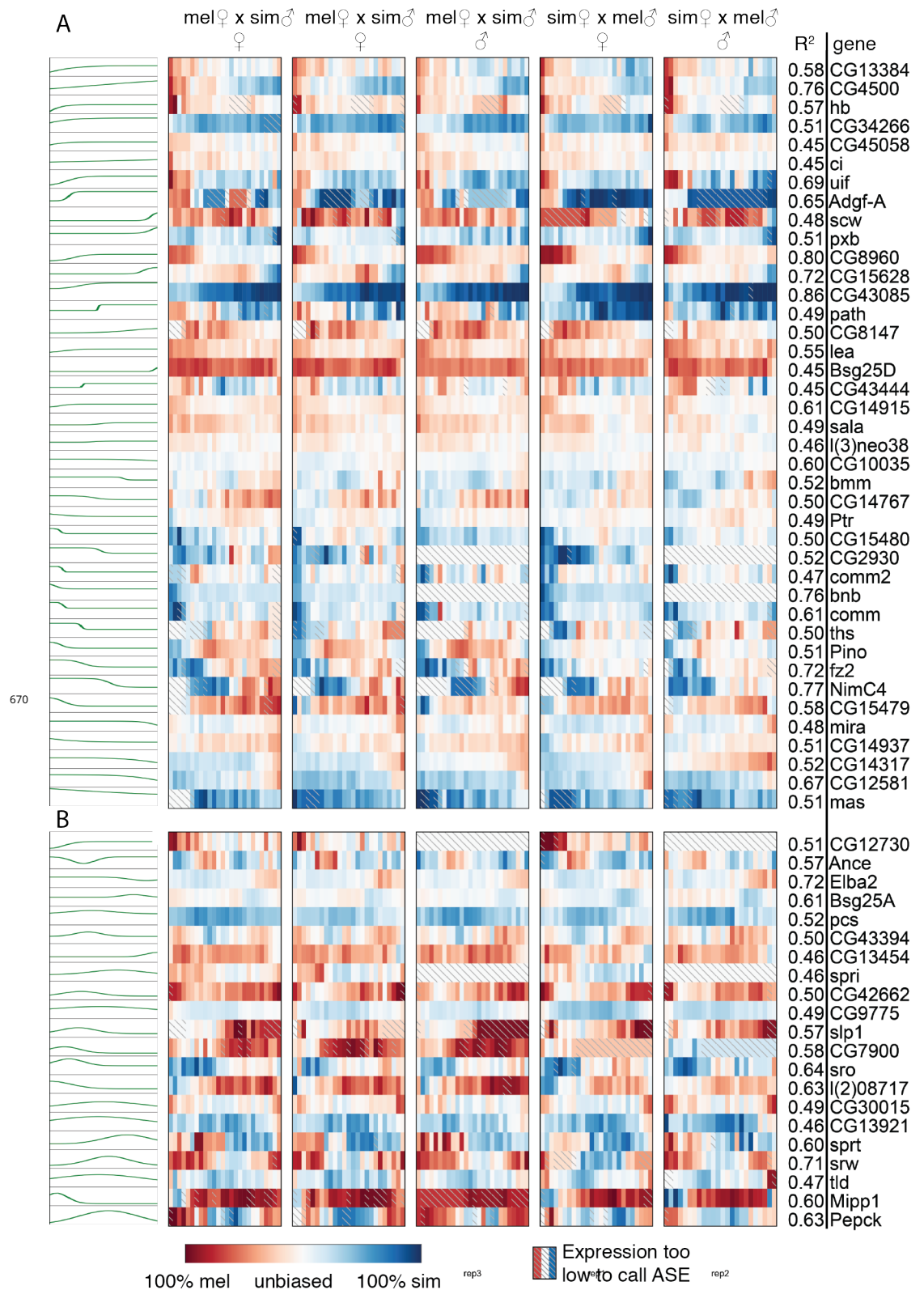
A) We used earth mover distance (EMD) to quantify the difference in patterns between each embryo. Given the green and pink patterns, EMD minimizes the amount of work that must be done to turn one pattern into the other. B) Hypothetical examples of pattern differences with low, intermediate, and high EMDs. C) Histograms of replicate hybrid embryos compared to each other (dark blue) and hybrid embryos compared to the average of splines fit on the parental embryos (cyan).

Figure 1-Figure supplement 2. Using earth mover distance to identify genes with different expression patterns between the hybrids and the parents



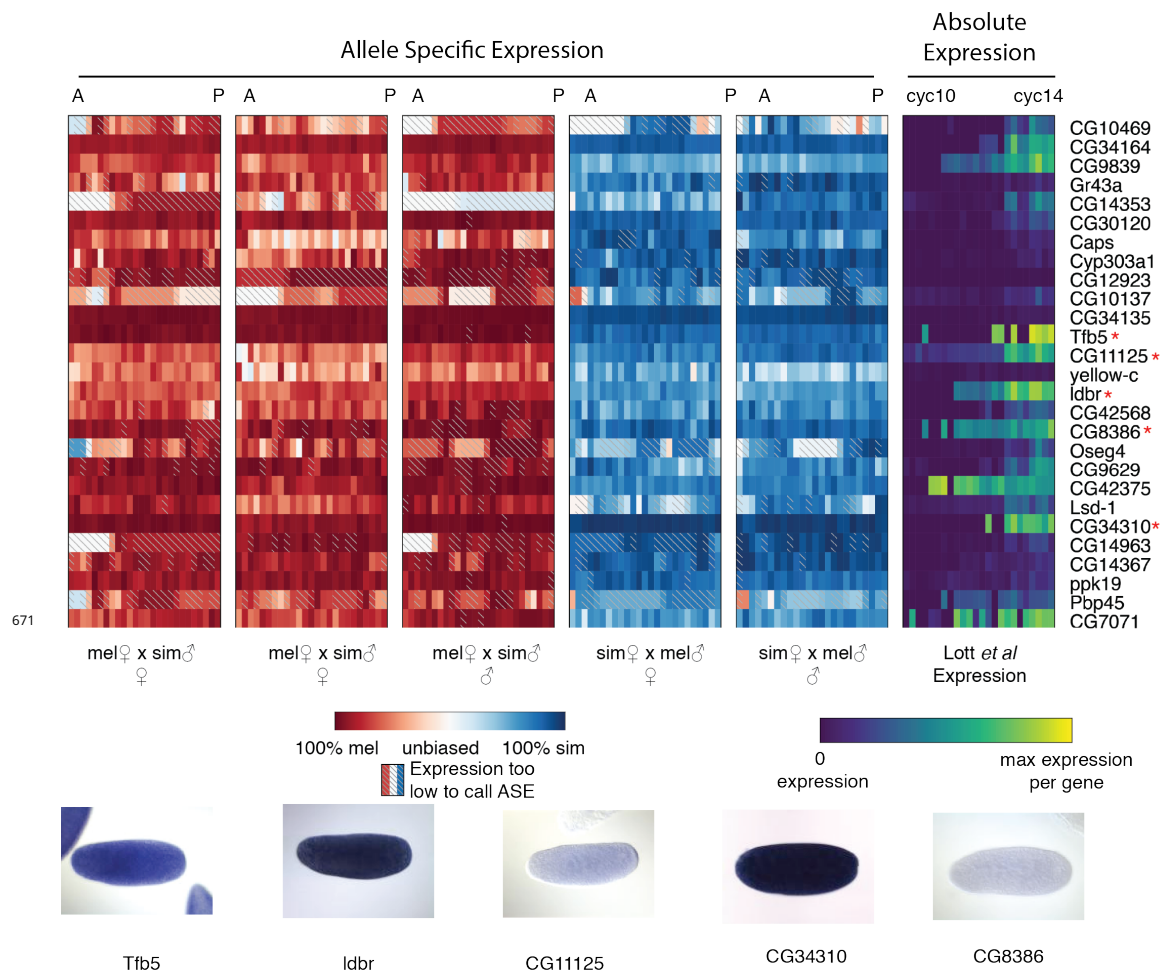
We found 171 genes with a significantly different EMD between each direction of the cross compared to replicates of each direction (Benjamini-Hochberg q-value < .05; *Benjamini and Hochberg (1995)*). The heatmap for each gene has each embryo aligned with anterior to the left and posterior to the right. Genes that are also significant after Bonferroni multiple testing correction are marked in red. We manually categorized these as due either to A) the embryos having clear parent of origin expression patterns that we interpret as due to species-specific maternal deposition (ASE data, not shown, generally supports this interpretation), B) a single embryo having a different expression pattern, marked with a red star, or C) more subtle expression differences or noise in expression measurement. Order within each class is arbitrary.

Figure 1-Figure supplement 3. Using earth mover distance to identify genes with different expression patterns between the directions of the hybrid cross



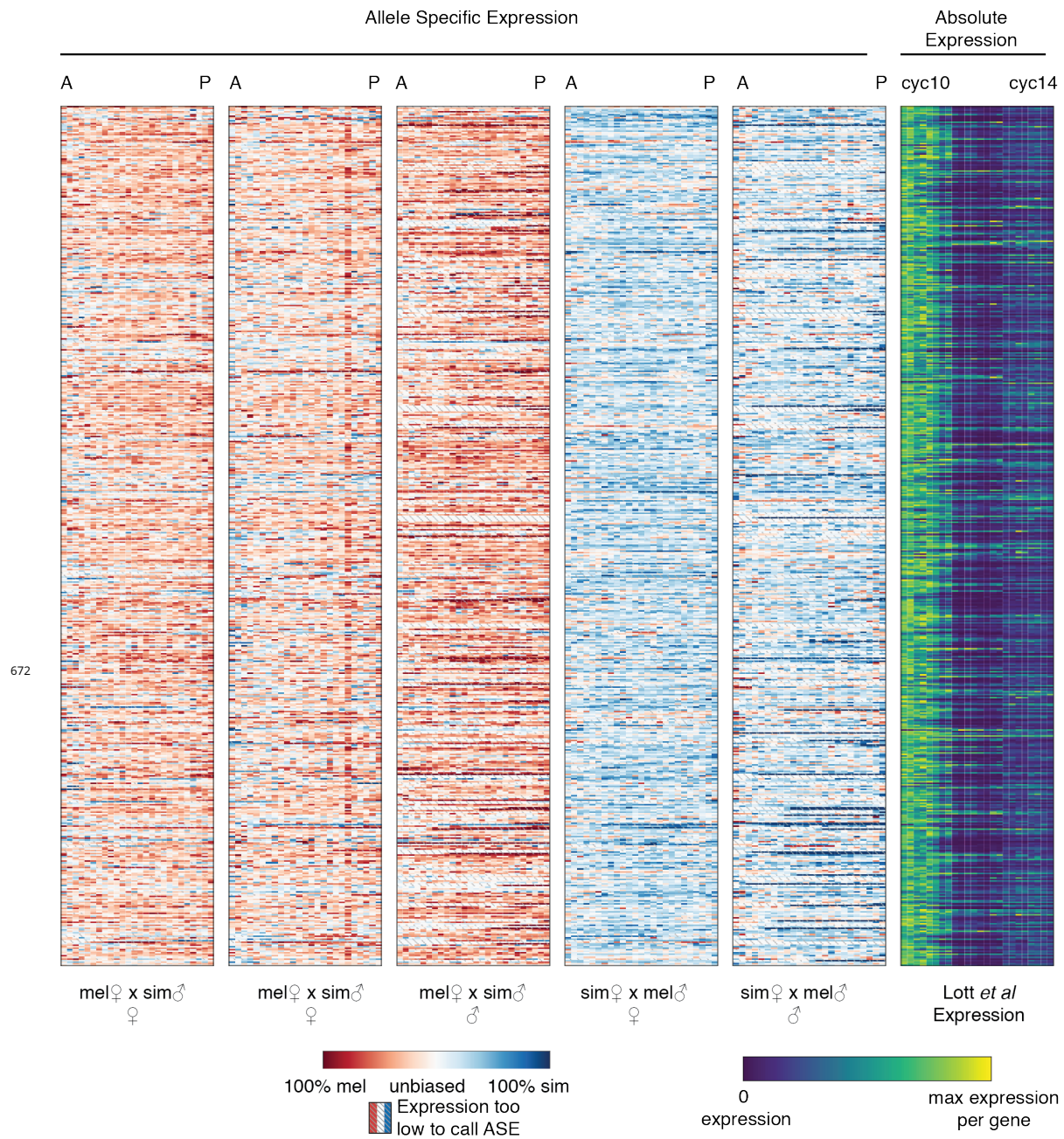
Genes from Figure 1B and C in the same order, but with the complete set of ASE data and R^2 values of the fit provided. A) Genes best fit by a logistic function and B) genes best fit by a normal function.

Figure 1-Figure supplement 4. Complete heatmap of ASE for genes with svASE.



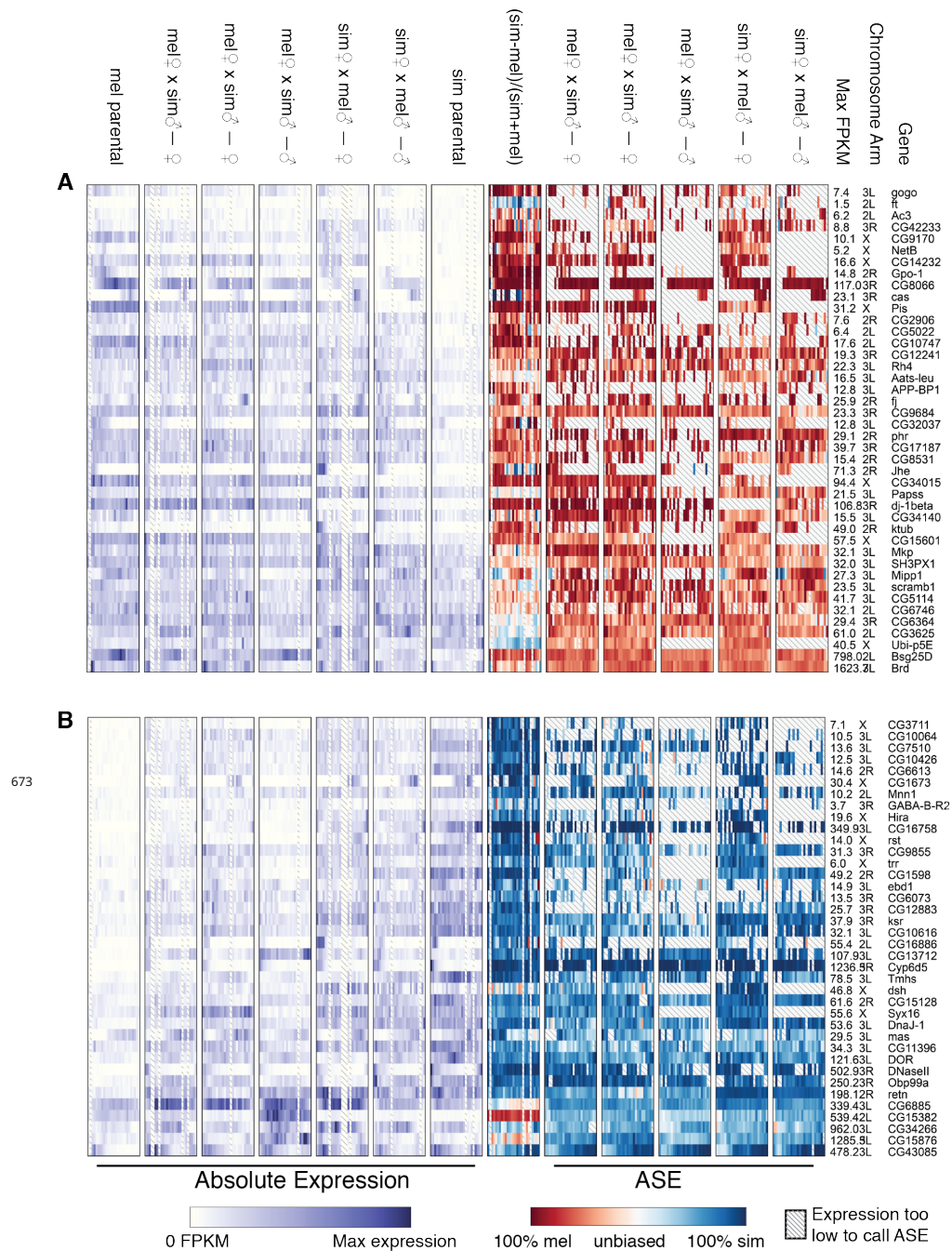
The left five columns indicate ASE from our hybrids, and the right column indicates RNA-seq expression in *Lott et al. (2011)*, with bright yellow indicating the larger of the highest expression for that gene in the dataset or 10FPKM. Of the 27 genes in this set, 13 have been assayed by the BDGP in *Tomančak et al. (2002)*, including the 5 shown with expression in the earliest time points, before most zygotic expression.

Figure 1–Figure supplement 5. Genes identified as maternally deposited in our data but as zygotically expressed in *Lott et al. (2011)*



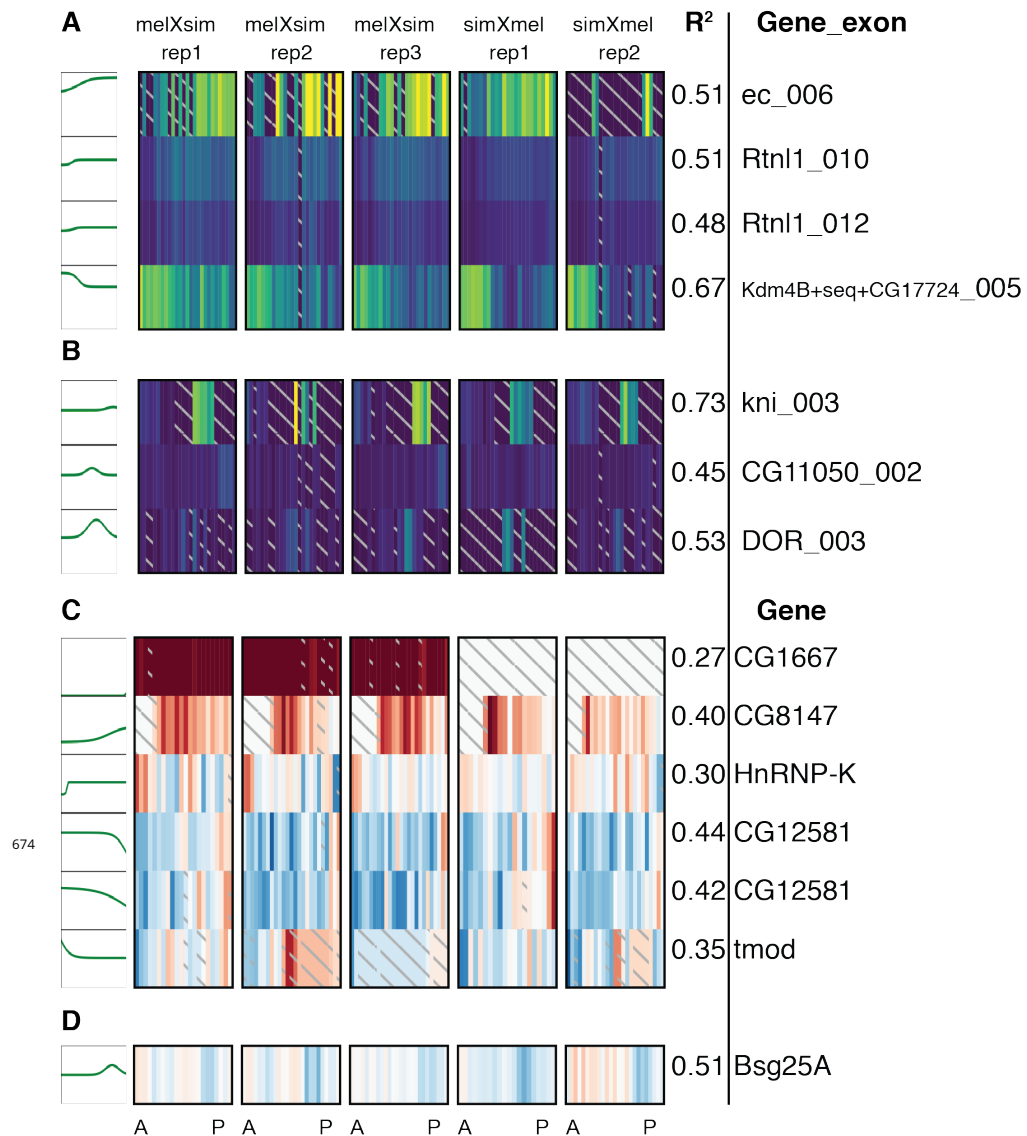
The left five columns indicate ASE from our hybrids, and the right column indicates RNA-seq expression in *Lott et al. (2011)*. Although there is clearly a maternal trend to the data, there is non-trivial zygotic expression in our data, and a slight increase in expression in the *Lott et al. (2011)* time course during cycle 14.

Figure 1–Figure supplement 6. Genes identified as zygotically expressed in both crosses in our data but maternally deposited in *Lott et al. (2011)*.



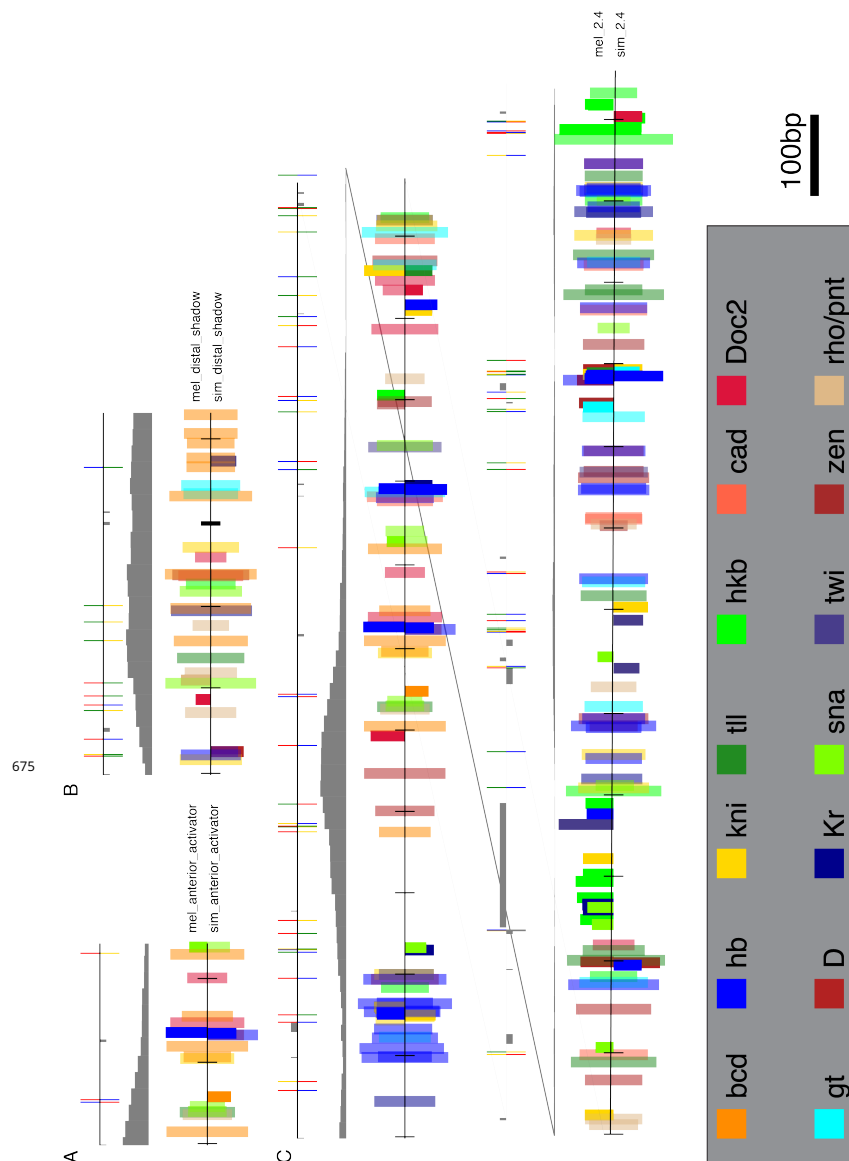
Genes strongly biased towards transcribing *D. melanogaster* (A) or *D. simulans* (B) alleles, regardless of whether *D. melanogaster* or *D. simulans* is the mother or father. Absolute expression values are normalized to the most highly expressed slice in each embryo (or 10 FPKM, whichever is higher). Genes are sorted by highest FPKM in the species that is un-expressed in the hybrid. The column (sim-mel)/(sim+mel) is the expected ASE assuming expression level is encoded in cis, and is computed by comparing matching slices of the parental embryos. ASE is not interpolated if there are not enough reads to call in a given slice.

Figure 1-Figure supplement 7. Genes with species-specific expression, regardless of parent of origin



A-B) Genes with spatially varying exon usage. We fit a step-like function (A) or a peak-like function (B) to the per-slice Percent Spliced In (PSI) value for each exon. DEXSeq combines the overlapping exons from *Kdm4B*, *seq*, and *CG17724* into a single unit since the UTRs of one gene are CDSs of others. C-D) Genes with spatially varying allele-specific splice-junction usage. Except for *bl*, the patterns are qualitatively similar to the spatially varying ASE. All heatmaps are arranged anterior to the left and posterior to the right. Green lines to the left of each gene heatmap are the best fit curve.

Figure 1-Figure supplement 8. Genes with spatially varying splicing.



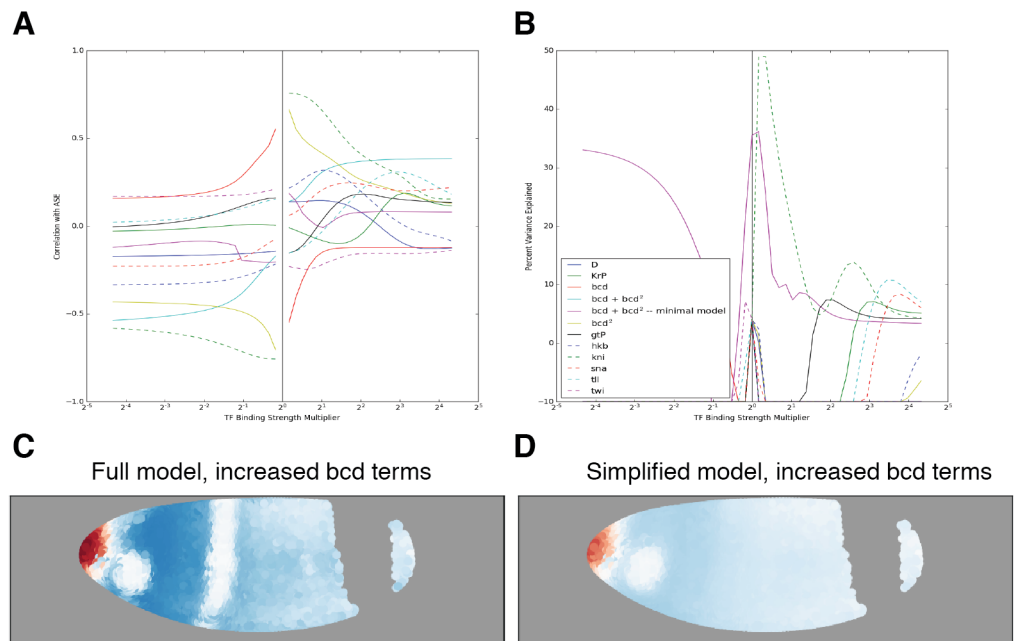
Positions of TF binding motifs in the canonical anterior CRM from *Driever and Nüsslein-Volhard (1989)* (A), the distal "shadow" CRM from *Perry et al. (2011)* (B), and the non-minimal 2.4kb CRM construct from (of which the canonical CRM is a subset) *Schröder et al. (1988)*, split across two lines for compactness. Within each CRM, the top line indicates the location of SNPs (colored lines) and insertions/deletions (grey bars on the side with the insertion) in a pairwise alignment of the two sequences. The middle track indicates DNase accessibility from *Thomas et al. (2011)*. The third track indicates the locations of FIMO motifs for a variety of TFs. TFs that have a motif with approximately equal strength ($\pm 20\%$) within 5bp have reduced opacity to better highlight motif changes. Bar height corresponds to FIMO score.

Figure 3-Figure supplement 1. Motif content of the CRMs for all TFs included in the model.

	β	std err	z	P> z	[95.0% Conf. Int.]
bcdP	69.3380	3.734	18.570	5.6×10^{-77}	62.020 76.656
bcdP2	-92.0808	5.249	-17.543	6.7×10^{-69}	-102.368 -81.793
twi	6.6254	1.610	4.115	3.9×10^{-05}	3.470 9.781
D	7.5322	0.659	11.432	2.9×10^{-30}	6.241 8.824
tll	-13.9656	1.379	-10.125	4.3×10^{-24}	-16.669 -11.262
h	-1.7576	0.736	-2.387	0.017	-3.201 -0.314
kni	-11.6206	0.787	-14.765	2.5×10^{-49}	-13.163 -10.078
hkb	-6.8310	2.364	-2.890	0.004	-11.464 -2.198
cad	-0.3796	1.673	-0.227	0.821	-3.659 2.900
gtP	-17.5613	0.824	-21.322	7.1×10^{-101}	-19.176 -15.947
sna	-11.8296	1.833	-6.455	1.1×10^{-10}	-15.421 -8.238
KrP	-11.5487	0.675	-17.109	1.3×10^{-65}	-12.872 -10.226
const	-0.3712	0.734	-0.506	0.613	-1.809 1.067

676

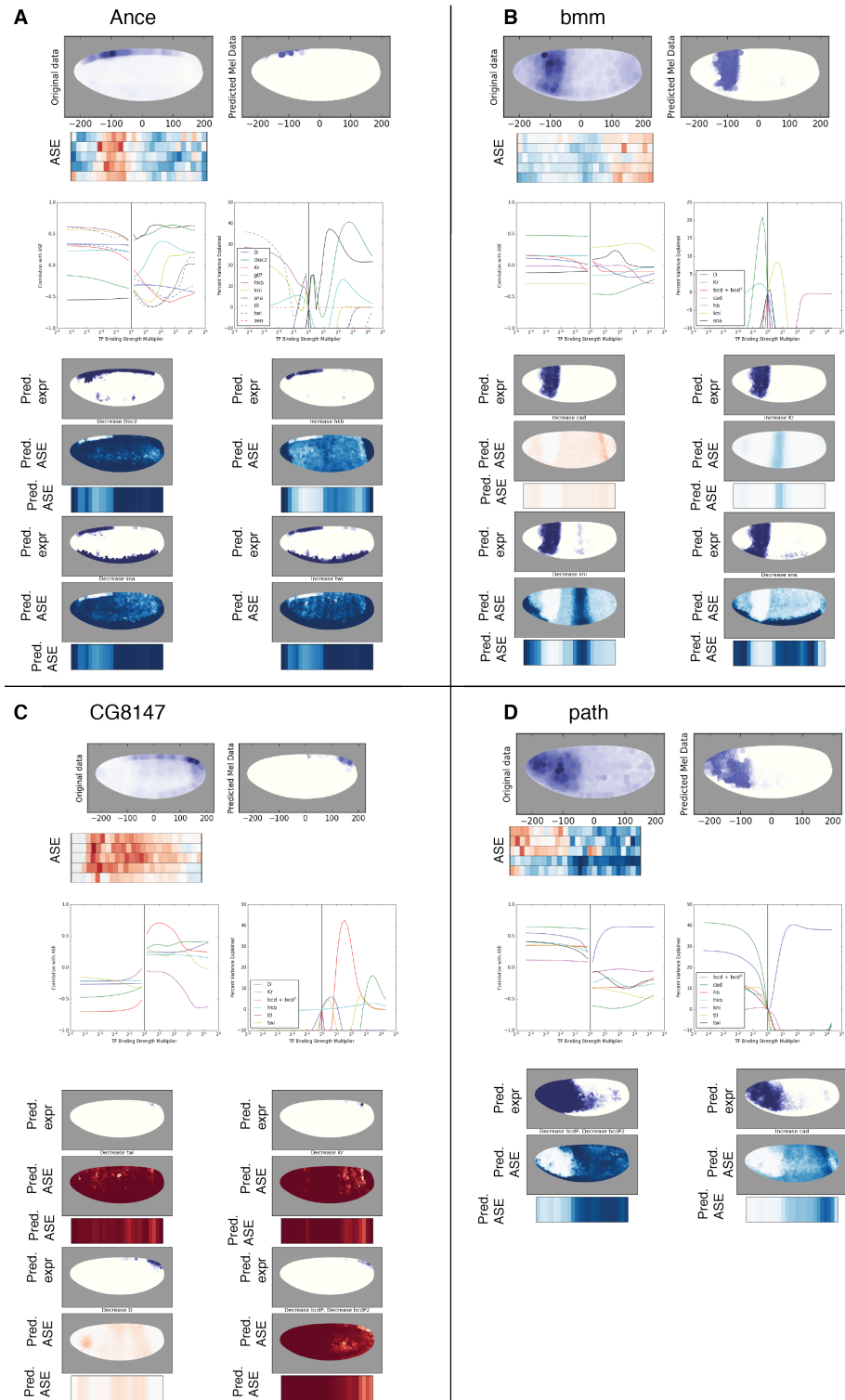
Figure 3–Figure supplement 2. Coefficients of the best-fit model for TFs bound near the anterior activator of *hb*



677

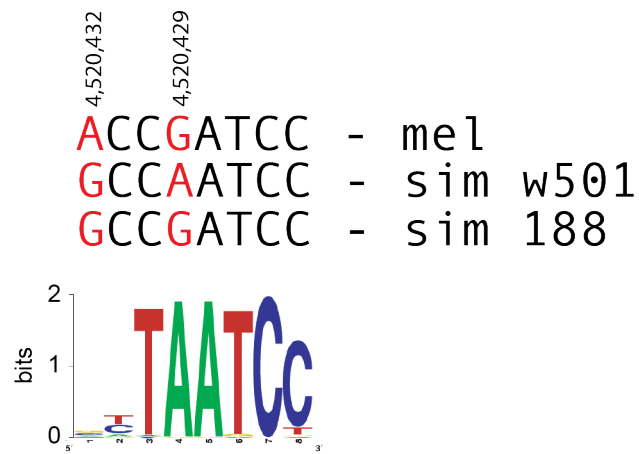
We altered each coefficient separately (with the exception of the Bicoid terms, which we also adjusted in tandem) by multiplying by a range of multipliers, then predicting ASE. Although increasing the Kni term in the model had the best correlation with the real ASE, there were no Kni motif changes in the known CRMs, so we excluded it from consideration. In addition, due to the buffering effects of the other TFs in the full model, we could not find a change that, when applied to both the Bcd and Bcd² term that explained the ASE; however, adjusting a simpler model consisting of only terms for Bcd, Bcd², *D*, and *twi* did yield a good fit. The actual predicted ASE for these models at a given change of coefficient is qualitatively very similar (C-D).

Figure 3–Figure supplement 3. Correlation of the predicted *hb* ASE with the real ASE (A) and percent of the variance explained by predicted ASE (B) at a range of coefficient strengths.

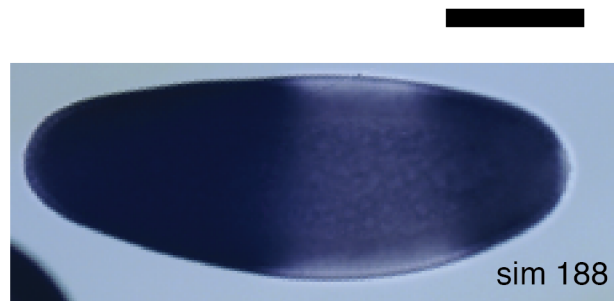


Modeling suggests plausible changes to the regulatory function that could generate the observed allele-specific expression. We fit a logistic model to the atlas expression, then adjusted each term of the model to find the coefficient that best matches the observed ASE in the slices (after setting mean ASE to match in the real and predicted data, since there may be mapping bias). The expression is then predicted in the adjusted model (purple embryo), which is also used to generate predicted ASE on a per-nucleus (red/blue embryo) and computationally sliced (heatmap) basis. Multiple TF changes can generate substantially similar sliced ASE data, while still having distinct expression patterns; *in situs* of the *D. simulans* embryos would be needed to distinguish between them.

Figure 3-Figure supplement 4. Proposed TF binding changes that generate svASE in *Ance*, *bmm*, *CG8147*, and *path*. We did not attempt modeling of the pair-rule genes *pxb*, *Bsg25A*, *comm2*, and *pxb*,



680



Scale bar 100 μ . Other bases in the region are identical to the reference *D. melanogaster* and *D. simulans* sequences.

Figure 4–Figure supplement 2. A naturally occurring strain of *D. simulans* with one of the base pair changes found in our edited line does not show the anterior gap of expression, closer to the *D. melanogaster* pattern.